A posttranscriptional pathway regulates cell wall mRNA expression in budding yeast

Cell Reports

Article

A posttranscriptional pathway regulates cell wall mRNA expression in budding yeast

Graphical abstract

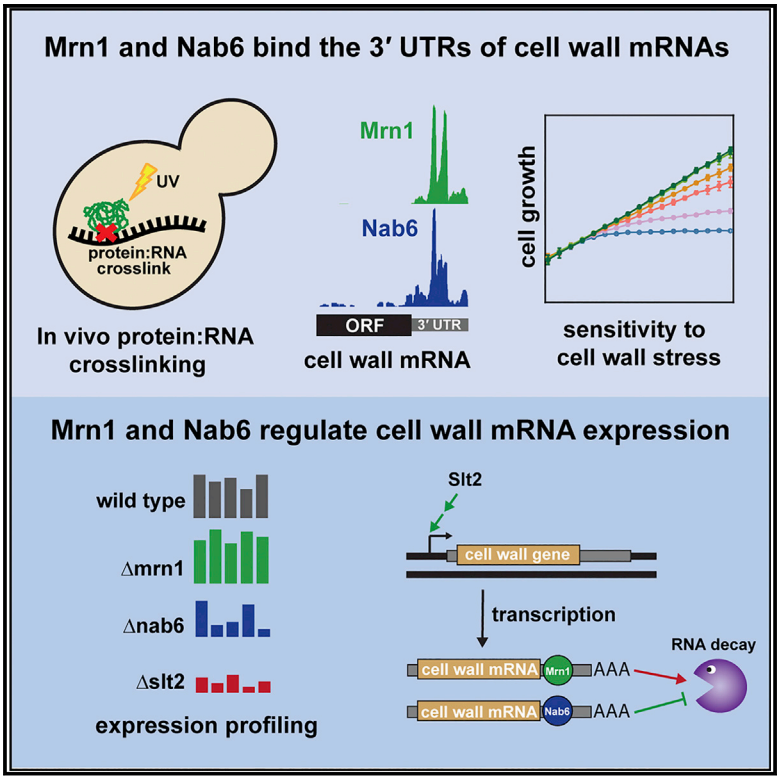

Highlights

- The RNA-binding proteins Mrn1 and Nab6 target cell wall-associated mRNAs
- Mrn1 and Nab6 act antagonistically to regulate cell wall mRNA expression
- Nab6 mediates resistance to antifungal compounds

Authors

Stefan Bresson, Vadim Shchepachev, David Tollervey

Correspondence

stefan.bresson@ed.ac.uk (S.B.), d.tollervey@ed.ac.uk (D.T.)

In brief

The cell wall is an important target for antifungal agents. Bresson et al. show that Nab6 and Mrn1 specifically bind cell wall mRNAs to regulate gene expression. Working together with the transcriptional cell wall integrity pathway, Nab6 mediates posttranscriptional responses to cell wall-damaging agents in budding yeast.

Bresson et al., 2023, Cell Reports *42*, 112184
March 28, 2023
https://doi.org/10.1016/j.celrep.2023.112184

CellPress

Cell Reports

CellPress
OPEN ACCESS

Article

A posttranscriptional pathway regulates cell wall mRNA expression in budding yeast

Stefan Bresson,[1,2,*] Vadim Shchepachev,[1,2] and David Tollervey[1,3,*]
[1]Wellcome Centre for Cell Biology and Institute of Cell Biology, School of Biological Sciences, University of Edinburgh, Edinburgh EH9 3BF, Scotland, UK
[2]These authors contributed equally
[3]Lead contact
*Correspondence: stefan.bresson@ed.ac.uk (S.B.), d.tollervey@ed.ac.uk (D.T.)
https://doi.org/10.1016/j.celrep.2023.112184

SUMMARY

The fungal cell wall provides protection and structure and is an important target for antifungal compounds. A mitogen-activated protein (MAP) kinase cascade termed the cell wall integrity (CWI) pathway regulates transcriptional responses to cell wall damage. Here, we describe a posttranscriptional pathway that plays an important complementary role. We report that the RNA-binding proteins (RBPs) Mrn1 and Nab6 specifically target the 3′ UTRs of a largely overlapping set of cell wall-related mRNAs. These mRNAs are downregulated in the absence of Nab6, indicating a function in target mRNA stabilization. Nab6 acts in parallel to CWI signaling to maintain appropriate expression of cell wall genes during stress. Cells lacking both pathways are hypersensitive to antifungal compounds targeting the cell wall. Deletion of *MRN1* partially alleviates growth defects associated with *Δnab6,* and Mrn1 has an opposing function in mRNA destabilization. Our results uncover a posttranscriptional pathway that mediates cellular resistance to antifungal compounds.

INTRODUCTION

Most organisms growing in the wild will frequently encounter a range of environmental stresses. This is particularly the case for budding yeasts that grow on the surface of plants, including fruits, grains, and bark. The fungal cell wall provides the primary physical barrier to the external environment and confers substantial protection against environmental insults. In *Saccharomyces cerevisiae*, the cell wall is comprised of an inner layer of branched β-1,3 glucan, β-1,6 glucan, and chitin and a covalently attached outer layer of mannoproteins.[1] The inner layer provides rigidity and structural support, while the outer layer allows the cell to interact with the external environment. Most components of the cell wall are unique to fungi and thus form common substrates for pathogen-associated pattern recognition receptors (PRRs) in plant and animal immune systems. For the same reason, the cell wall is an attractive target for antifungal drugs. The echinocandin family of compounds, including caspofungin, inhibits β-1,3 glucan synthase.[2] Other antifungal compounds such as Congo red and Calcofluor white seem to disrupt cell wall structure by binding chitin and β-glucan polymers.[3,4]

The major signaling pathway regulating cell wall growth and homeostasis is the cell wall integrity (CWI) pathway.[5] Damage to the cell wall is detected by several sensor proteins (Wsc1-3, Mid2, and Mtl1) located in the plasma membrane. These stimulate the GEF/GTPase pair Rom2 and Rho1, which in turn activate the Pkc1 kinase. Pkc1 initiates a mitogen-activated protein kinase (MAPK) cascade consisting of Bck1, Mkk1/Mkk2, and Slt2. Ultimately, Slt2 launches a transcriptional response via the transcription factor Rlm1 and the chromatin modifiers SWI/SNF and SAGA.[6,7] Slt2 also regulates transcription directly by phosphorylating Tyr1 residues in the C-terminal domain of RNA polymerase II,[8] the Mediator complex subunit Med13,[9] and the cyclin C Ssn8.[10,11] CWI signaling is supplemented by the high-osmolarity glycerol (HOG) pathway, which responds to a subset of cell wall stresses, most notably zymolyase treatment.[12,13]

Posttranscriptional pathways may provide an additional layer of regulation in cell wall biosynthesis and/or integrity.[14] A previous RNA-immunoprecipitation and microarray screen identified several RNA-binding proteins (RBPs), including Bfr1, Hek2, Mrn1, Nab6, Pub1, Scp160, and Ssd1, that preferentially associate with cell wall-related mRNAs.[15] The best characterized of these proteins is Ssd1, which represses translation initiation of specific cell wall mRNAs, probably via its interactions with the 5′ UTRs of these transcripts.[16–18] Notably, the *ssd1Δ* knockout confers sensitivity to compounds targeting the cell wall[16,17,19] and synergistically impairs growth when combined with mutations in the CWI pathway.[20] Other RBPs targeting cell wall mRNAs have not yet been investigated in detail but may have similar roles in regulating cell wall growth and integrity.

We previously assessed changes in global RNA-protein interactions following a variety of stresses using total RNA-associated proteome purification (TRAPP).[21,22] Among the proteins

showing stress-induced changes in RNA binding were the putative cell wall regulators Mrn1 and Nab6. To better understand their roles, we characterized the RNA targets for Mrn1 and Nab6. We report that both proteins specifically target the 3′ UTRs of a largely overlapping group of cell wall-related mRNAs but have antagonistic effects on gene expression.

RESULTS

Mrn1 and Nab6 are related proteins with similar domain architectures

Mrn1 is relatively well conserved throughout most major fungal lineages (Figure S1A); Nab6, by contrast, is found in only a subset of ascomycete yeasts and is generally less well conserved (Figure S1B). Nab6 and Mrn1 are predicted to contain two and four RNA-recognition motifs (RRMs), respectively (Figure 1A). By analyzing the AlphaFold prediction for Nab6,[23,24] we identified two additional RRMs (designated "putative" and shown in blue and white stripes) that show robust structural homology to a conventional RRM (Figures 1A and S1C–S1F). A BLAST search for Nab6 homologs across the *S. cerevisiae* genome returned Mrn1 as the top hit, and vice versa, suggesting a close evolutionary relationship between the two proteins. Further analysis revealed that Nab6 and Mrn1 share a region of homology encompassing RRM3 and RRM4 in each protein (Figures S1G–S1H). Taken together, these observations suggest that both proteins likely function through direct RNA binding and possibly share related functions and/or RNA targets.

Mrn1 and Nab6 target the 3′ UTRs of cell wall-related mRNAs

To identify the RNA targets of Mrn1 and Nab6, we mapped their RNA binding sites using CRAC (crosslinking and amplification of cDNA).[25] Mrn1 and Nab6 were separately expressed as C-terminal HF-tagged (His_8-Ala_4-FLAG) fusion proteins under the control of their endogenous promoters (Figure 1A). The resulting strains were grown to the exponential phase and UV irradiated to covalently fix direct protein-RNA contacts. Subsequently, RNAs associated with Mrn1 or Nab6 were isolated using tandem affinity purification, treated with RNase to generate protein-protected RNA footprints, and analyzed by high-throughput sequencing.

We first examined the distribution of sequencing reads across 5′ UTR, coding region, and 3′ UTR sequences (Figure 1B). Mrn1 and Nab6 preferentially bound 3′ UTRs; these formed 65% and 41% of CRAC reads, respectively, compared with just 8% of total RNA sequencing (RNA-seq) reads. As a control, we analyzed CRAC reads derived from the translation initiation factor eIF4B, which was also HF tagged.[21] As expected, eIF4B was strongly enriched at 5′ UTRs and showed negligible binding to 3′ UTRs (Figure 1B).

Mrn1 and Nab6 reproducibly bound a relatively small set of transcripts (Figures 1C–1E; Table S1), with substantial overlap in their targets. Both proteins bound a core set of mRNAs encoding cell wall components (highlighted in yellow), including *HSP150*, *SED1, CWP2*, *ASP3*, and *SCW4*, among others. Indeed, the primary Gene Ontology (GO) terms associated with Mrn1 and Nab6 targets were related to the cell wall (Figure S2A). Mrn1 additionally targeted *RPI1*, encoding a transcription factor for cell wall proteins.[26] The most enriched Nab6 target was *YDR524C-B*. Although designated as an uncharacterized gene, YDR524C-B shows strong genetic interactions with various cell wall factors (Figure S2B).[20] In addition to cell wall-related mRNAs, several other targets were identified (Figures 1C–1E), including transcripts for plasma membrane proteins (highlighted in green). Mrn1 also targeted *RNR1*, encoding ribonucleotide reductase, and both Mrn1 and Nab6 bound *SML1*, encoding an Rnr1 inhibitor (both highlighted in pink). Another prominent target for both Mrn1 and Nab6 was *MFA1*, encoding a secreted mating pheromone. Mrn1 also bound its own mRNA but within the 5′ UTR, which was indicative of possible autoregulation (Figure S2C).

RBPs often interact promiscuously with a wide range of transcripts. However, comparing representation in CRAC with mRNA abundance measured by RNA-seq indicated that Mrn1 and Nab6 show surprisingly high specificity for their mRNA targets (Figure 1D; Table S1). For example, reads mapping to the *HSP150* mRNA comprised ~5% of the Mrn1 and Nab6 CRAC libraries but only 0.15% of all mRNA reads. Moreover, cell wall mRNAs, as a class, were highly overrepresented in both CRAC datasets (Figure S2D).

Finally, we examined the distribution of Mrn1 and Nab6 binding across individual transcripts (Figures 1F and S2C). Each protein mostly targeted the 3′ UTR region, usually at a single site. Interestingly, the Mrn1 and Nab6 binding sites sometimes coincided (e.g., *HSP150* and *SED1*). There is no reported evidence for direct physical interaction between Mrn1 and Nab6 (Saccharomyces Genome Database), suggesting that the two proteins may compete for binding to some target transcripts.

Loss of Nab6 confers sensitivity to cell wall damage

Given their clear association with cell wall-related mRNAs, we tested whether disrupting Mrn1 and/or Nab6 function sensitizes yeast to cell wall damage. Two major signaling pathways detect and respond to cell wall damage (Figure 2A). Congo red (CR), caspofungin (CSF), and Calcofluor white (CFW) activate the CWI MAPK cascade that includes Bck1 and Slt2. Zymolyase, a mixture of cell wall-degrading enzymes, elicits a response via sequential activation of HOG and Slt2.[5,12,27]

We generated *Δmrn1* and *Δnab6* single mutants and a *Δmrn1 Δnab6* double-deletion strain, either alone or in combination with deletions in the CWI (*Δslt2* or *Δbck1*) and HOG (*Δhog1*) pathways (Figure 2A). Individual deletion strains grew normally, but loss of both Nab6 and CWI pathway components (*Δnab6 Δbck1* and *Δnab6 Δslt2*) gave a clear synthetic growth defect (Figure 2B). To examine whether Nab6 and/or Mrn1 are involved in cell wall stress response, each strain was challenged with low and high doses of the cell wall-damaging agent CR (Figure 2B). Low-dose CR (0.5 μg/mL) did not impair growth of the individual knockout strains but was lethal for the *Δnab6 Δbck1* and *Δnab6 Δslt2* strains. To confirm that the cells were inviable due to compromised CWI, we repeated the experiment using growth medium supplemented with 1 M sorbitol, which provides osmotic support to prevent cell lysis. Notably, sorbitol completely rescued the hypersensitivity of the *Δnab6 Δbck1* and *Δnab6 Δslt2* strains to 0.5 μg/mL CR (Figure S3).

CellPress
OPEN ACCESS

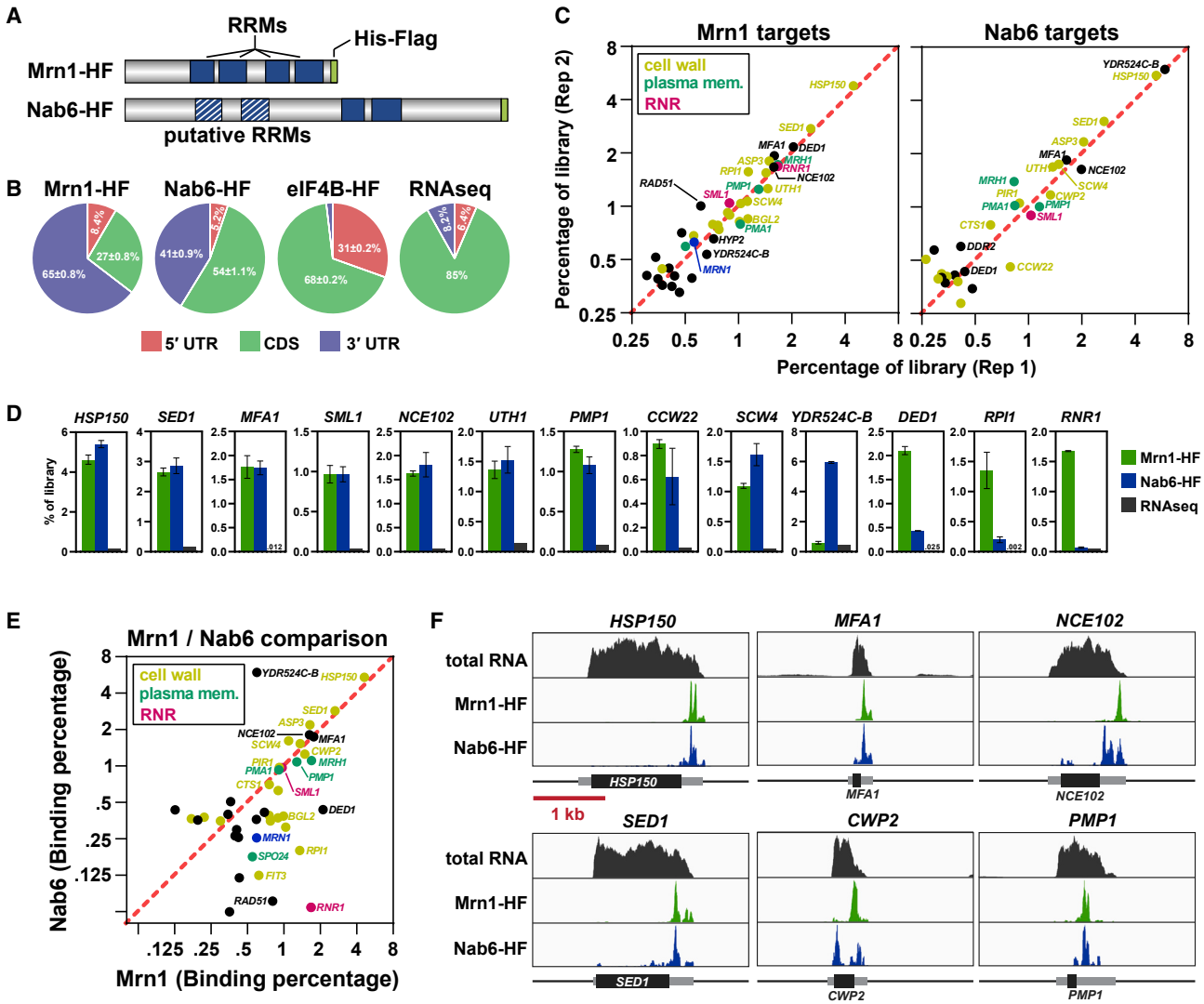

Figure 1. Transcriptome-wide identification of Mrn1 and Nab6 targets

(A) Domain architecture of Mrn1 and Nab6. Two putative RRMs identified using AlphaFold are shown in blue and white stripes. Each protein was tagged with His_8-FLAG at the C terminus.

(B) Distribution of Mrn1, Nab6, and eIF4B binding to the 5′ UTR, CDS, and 3′ UTR regions of target RNAs. RNA-seq data are included as a control.

(C) Scatterplots showing the top mRNA targets of Mrn1 (left) and Nab6 (right). Each plot includes all genes comprising at least 0.35% of mRNA-mapped reads. See Table S1 for a complete list of target transcripts. Proteins related to the "cell wall," "plasma membrane," or ribonucleotide reductase ("RNR") are indicated. Annotations were manually curated from the literature.

(D) Bar graphs showing the percentage of reads in each library that map to selected transcripts. Error bars show standard deviation of the mean (n = 2).

(E) Comparison of the top targets of Mrn1 and Nab6.

(F) Binding of Mrn1 and Nab6 across shared target transcripts. Each track is normalized to total library size using reads per million. RNA-seq reads are included as a control. Each box represents a 3 kb window; a scale bar is shown at the bottom. The open reading frames (ORFs) are shown as black boxes, with UTRs as flanking gray boxes. Each transcript is oriented 5′-3′.

At higher concentrations of CR (60 μg/mL), inactivation of the CWI pathway alone was lethal unless the cells were provided with osmotic support (Figures 2B and S3, compare row 1 with 5 and 9). By contrast, the *Δnab6* strain was viable but substantially growth impaired (Figure 2B, compare rows 1 and 3). Simultaneous deletion of Nab6 and the CWI pathway (*Δnab6 Δslt2* and *Δnab6 Δbck1*) was lethal with 60 μg/mL CR and could not be rescued with sorbitol (Figures 2B and S3A, rows 7 and 11).

Somewhat surprisingly, the individual *Δmrn1* knockout showed no discernable phenotype following CR treatment (Figure 2B, compare rows 1 and 2). However, *MRN1* showed a clear epistatic relationship with *NAB6*. Deletion of *MRN1* partially rescued the slow-growth phenotype of the *Δnab6* strain at

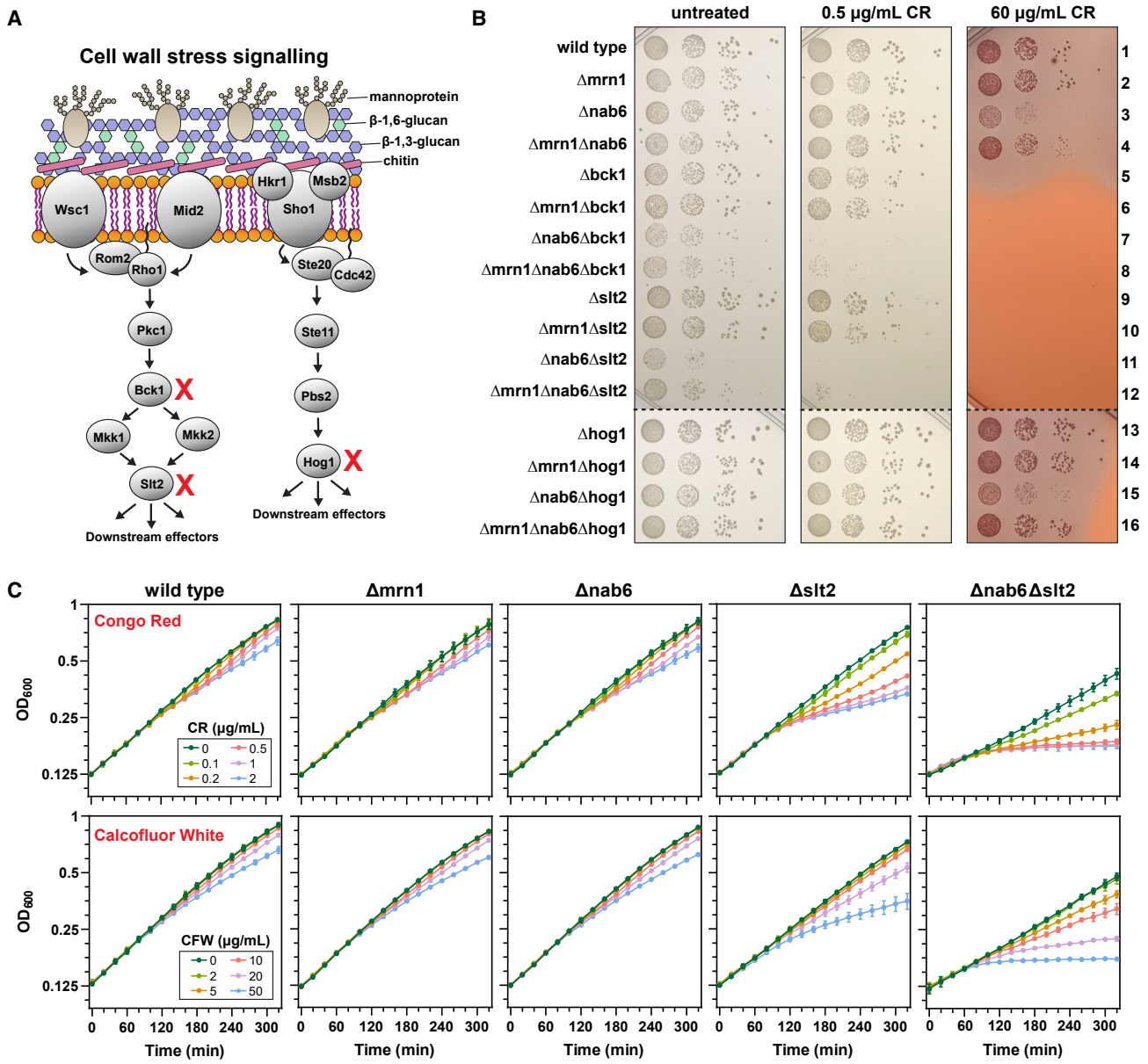

Figure 2. Nab6 acts in parallel to CWI signaling

(A) Schematic outline of the major cell wall stress signaling pathways. The cell wall integrity (CWI) pathway (left) responds to Congo red, Calcofluor white, caspofungin, and zymolyase, while the HOG pathway (right) responds to zymolyase. Genes deleted in (B) and (C) are marked with a red X.

(B) Strains with combinations of gene deletions were tested for their ability to grow on 0.5 and 60 μg/mL Congo red. Cells were grown for 2 days at 30°C.

(C) Growth curves for wild-type, *Δmrn1*, *Δnab6*, *Δslt2*, and *Δnab6 Δslt2* strains following treatment with increasing concentrations of Congo red (top) or Calcofluor white (bottom). Each point shows the mean (n = 2), and error bars indicate standard deviation. For some points, the error bars are too small to be visible.

high-dose CR (Figure 2B, compare rows 3 and 4 and 15 and 16), as well as the lethality observed for the *Δnab6 Δbck1* and *Δnab6 Δslt2* strains at low-dose CR (Figure 2B, compare rows 7 and 8 and 11 and 12).

Next, we repeated the growth tests in the presence of CSF, an antifungal drug that inhibits the activity of β-1,3-glucan synthase.[2] The individual *Δmrn1* and *Δnab6* strains grew normally, while inactivation of the CWI pathway (*Δbck1* or *Δslt2*) gave a slight growth defect (Figure S4). However, loss of both Nab6 and the CWI pathway (*Δnab6 Δbck1* and *Δnab6 Δslt2*) resulted in a severe synthetic growth defect. Importantly, growth was restored when the medium was supplemented with 1 M sorbitol, confirming that the source of the growth defect was compromised cell integrity.

To analyze growth kinetics in greater detail, we repeated some of the above experiments in liquid medium using various

concentrations of CR (Figure 2C). Wild-type cells and individual knockouts were moderately sensitive to CR, while the *Δnab6 Δslt2* strain was inviable at CR concentrations ≥0.5 μg/mL. Notably, the response to CR was not immediate. Wild-type cells and individual knockouts were modestly impaired beginning ~100–120 min posttreatment, while the *Δnab6 Δslt2* strain was inhibited by ~80 min. We attribute this to the progressive accumulation of cell wall damage during growth and division. We observed similar growth defects when cells were treated with CFW, an alternative cell wall-damaging agent. The individual *Δmrn1* and *Δnab6* strains responded similarly to wild type, while the *Δslt2* strain was moderately inhibited at higher doses (Figure 2C, bottom). By contrast, the *Δnab6 Δslt2* strain was completely inviable at concentrations >50 μg/mL.

Based on these results, we propose that Nab6 acts in parallel to the CWI pathway to maintain resistance to the increased cell wall stress generated by CR, CFW, and CSF. The more severe phenotype observed for *Δslt2* compared with *Δnab6* suggests that the CWI pathway mediates the primary response, while Nab6 plays an important supporting role. The related Mrn1 protein has overlapping RNA targets with Nab6 and a partially antagonistic role in responding to cell wall stress caused by CR.

Nab6 and Slt2 are required for full expression of cell wall mRNAs

Using the growth assays as a guide, we prepared a series of RNA-seq libraries from cells exposed to CR (Figure 3A). Poly(A)-selected RNA from wild-type, *Δmrn1*, *Δnab6*, *Δslt2*, and *Δnab6 Δslt2* cells was harvested under standard conditions ("time 0") or following treatment with low-dose CR (2 μg/mL) for 1, 2, and 4 h. In parallel, we treated wild-type, *Δmrn1*, *Δnab6*, and *Δmrn1 Δnab6* cells with high-dose CR (60 μg/mL) and harvested RNA after 2 h. Overall, replicate libraries were highly reproducible (Figure S5).

In untreated cells (Figure 3B), only four transcripts showed significant differential expression between *Δmrn1* and wild-type cells ($p < 0.01$). The most significantly upregulated transcript, *RAD51*, was also a strong Mrn1 binding target (highlighted in red in Figure 3B; see also Figures 1C and 1E). As a group, Mrn1 CRAC targets were mildly upregulated compared with non-targets, suggesting reduced stability from Mrn1 binding (Figure 3C). In the *Δnab6* strain, 9 transcripts were significantly downregulated, and 6 of these were also strong Nab6 CRAC targets (Figure 3B). The most significantly altered transcript was *SED1*, encoding a major stress-induced structural component of the cell wall.[28] Overall, Nab6 targets were substantially reduced in abundance compared with non-target transcripts in *Δnab6* (Figure 3D), indicating that Nab6 binding results in mRNA stabilization. Notably, the individual *Δsed1* strain was not impaired by CR (Figure S6A), suggesting that the sensitivity of *Δnab6* to cell wall stress is caused by the simultaneous depletion of multiple cell wall-related mRNAs (e.g., *HSP150*, *SED1*, *SCW4*, *PIR1*, etc.).

The *Δslt2* strain had relatively few differentially expressed genes compared with the wild-type strain (Figure 3B). As with *Δnab6*, the most significantly altered transcript was *SED1*, but several additional cell wall mRNAs were also downregulated, including *BGL2*, encoding Endo-β-1,3-glucanase, a key enzyme in cell wall synthesis and remodeling. The combined *Δnab6 Δslt2* strain showed a further decrease in cell wall mRNAs compared with either single deletion (Figure 3B), suggesting that Nab6 and Slt2 act independently to maintain normal levels of cell wall mRNAs.

We next determined the effects of CR. To our surprise, the different CR treatments (2 and 60 μg/mL) induced nearly identical changes in the transcriptome (Figure S6B). We therefore focused on the 2 μg/mL dose for subsequent analysis. Initially, we used principal-component analysis (PCA) to compare the global mRNA expression patterns for each strain throughout the time course (Figure 3E). The wild-type and *Δmrn1* strains showed similar profiles; *Δnab6* was more distinct but followed the same general trend. By contrast, the *Δslt2* strain showed a substantially altered response to CR, and this was even more marked in the *Δnab6 Δslt2* strain.

To further investigate this observation, we divided the mRNAs into eight clusters based on their response to CR in wild-type cells (Figure 3F; Table S3). Transcripts from clusters 1–3 (n = 4,408) were largely unchanged throughout the time course and were grouped together for subsequent analyses. The remaining mRNAs (n = 592) fell into one of five clusters based on their response profile. Cluster 5 mRNAs (n = 366) were modestly decreased, while mRNAs in clusters 4, 6, and 8 (n = 215) were all upregulated but with varying kinetics. Cluster 7 transcripts (n = 11) were strongly upregulated between 0 and 1 h posttreatment, plateaued between 1 and 2 h, and decreased thereafter. *SLT2* deletion markedly reduced, but did not completely abolish, the changes in transcript levels observed in clusters 4 through 8 (Figure 3F, middle and bottom panels). Additional loss of Nab6 further muted the response to CR. This was visible for genes in clusters 4–8 but was most apparent for cluster 4 and particularly the strong Nab6 targets *HSP150* and *SED1* (Figures S7A and S7B).

The *Δnab6 Δslt2* strain cannot grow in the presence of low-dose CR, even though the individual deletion strains are viable (Figure 2). To understand the molecular basis for this phenotype, we compared the transcriptomic profile of the *Δnab6 Δslt2* double mutant with the *Δslt2* single mutant (Figure 4). Several transcripts were downregulated in *Δnab6 Δslt2* cells compared with *Δslt2*, most of which were also direct binding targets for Nab6 (highlighted in red). Overall, these results are consistent with previous reports that the CWI pathway plays a major role in transcriptional reprogramming during cell wall stress[6,29] but support a parallel function for Nab6.

Loss of Mrn1 partially rescues molecular defects associated with the *Δnab6* strain

The growth tests revealed that Mrn1 is partially epistatic to Nab6 upon treatment with CR (Figure 2). To identify a molecular basis for this phenotype, we compared the *Δmrn1 Δnab6* double mutant with the *Δnab6* single mutant in the absence or presence of high-dose CR. Only a small number of transcripts were differentially expressed between the two strains (Figures 5A and 5B). However, two of these mRNAs (*SED1* and *BGL2*) encode important cell wall components and are bound by Nab6 and Mrn1 (Table S1). In unstressed cells, both transcripts were downregulated in the absence of Nab6, but mRNA levels were restored in

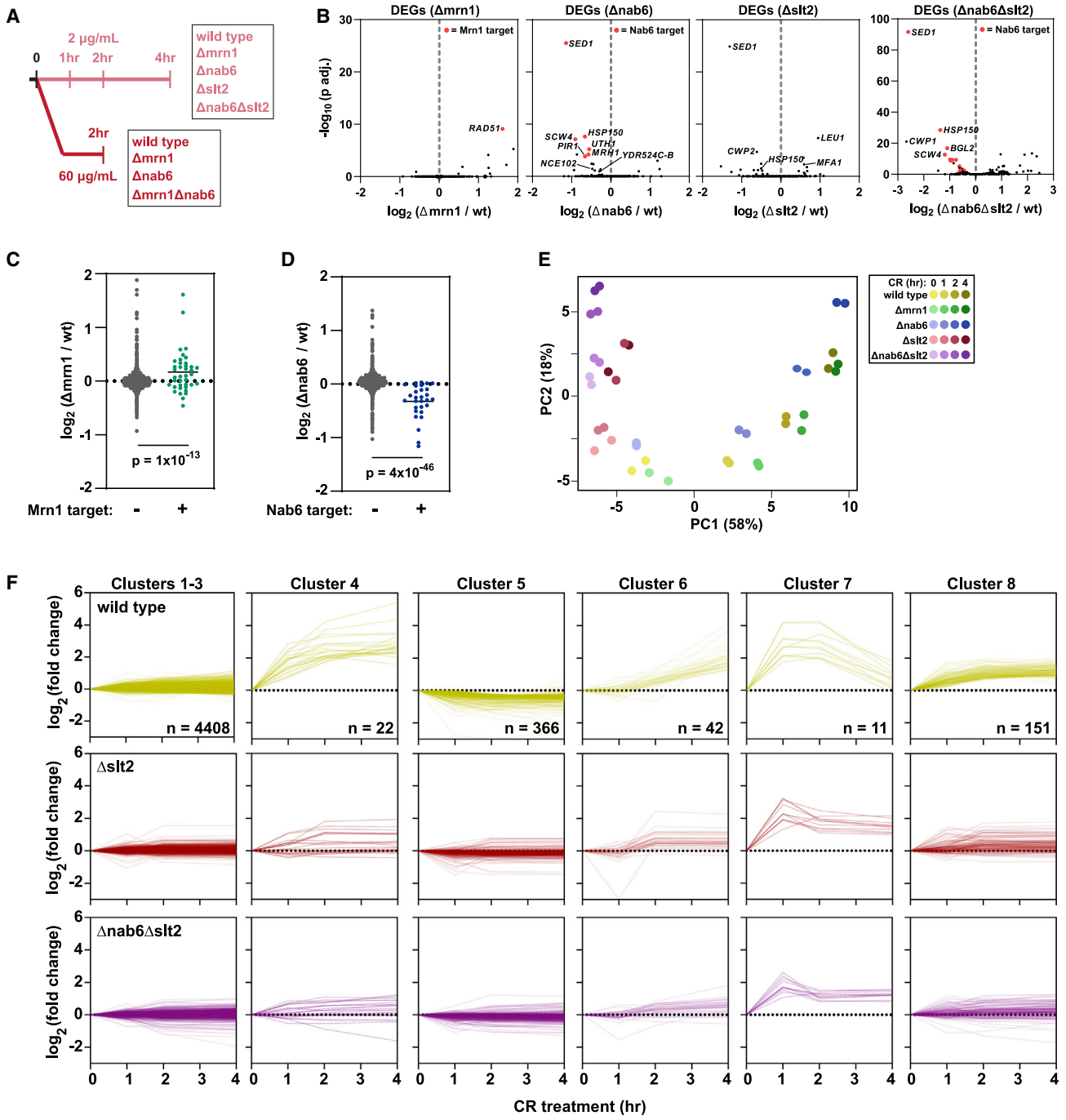

Figure 3. Nab6 positively regulates target mRNAs

(A) Schematic showing the overall design of the transcriptomic experiments. See text for details.

(B) Volcano plots showing differentially expressed genes between wild-type cells and various knockout strains. Transcripts that are significantly altered (p adj. < 0.01) and also a CRAC target of either Mrn1 or Nab6 are colored red. Adjusted p values were calculated using DESeq2.

(C) Scatterplots showing the difference in transcript levels between *Δmrn1* and wild-type cells. Transcripts are divided into Mrn1 CRAC targets (right) and non-targets (left). The solid black lines show the mean change in transcript levels. The p value was calculated using a two-sample t test.

(D) Same as (C) but for Nab6.

(E) PCA for different replicates, time points, and strains.

(F) Clustering of transcript expression profiles for wild-type cells following CR treatment. Expression profiles for the same genes are shown below for the *Δslt2* and *Δslt2 Δnab6* strains. Note that each plot shows results from the 0, 1, 2, and 4 h time points.

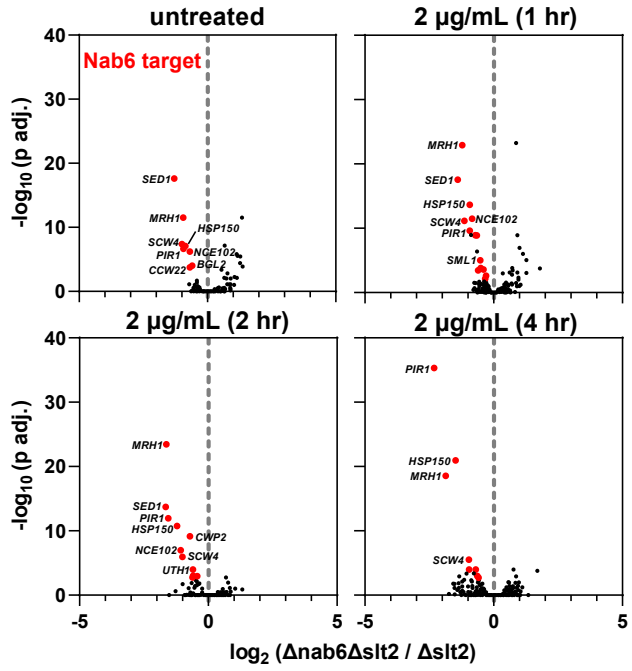

Figure 4. Loss of SLT2 exacerbates the expression defects associated with *Δnab6*

Volcano plots showing differentially expressed genes between *Δnab6 Δslt2* knockout strains and the *Δslt2* single mutant. Transcripts that are significantly altered (p adj. < 0.01) and also a CRAC target of Nab6 are colored red. Adjusted p values were calculated using DESeq2.

the double mutant. CR treatment increased the abundance of *SED1* and *BGL2* (note differences in scales) but did so to a lesser extent in the *Δnab6* strain (Figure 5C). Notably, additional deletion of Mrn1 once again rescued expression of *SED1* and *BGL2*. These findings support the model that Nab6 and Mrn1 have opposing roles in regulating the abundance of mRNAs encoding major cell wall proteins.

The predominant binding of Nab6 and Mrn1 to mRNA 3′ UTRs, including that of *SED1*, suggested that this region would be required for regulation by these proteins. To test this, we generated a reporter construct in which the coding sequence (CDS) for the fluorescent protein Venus was flanked by the promoter and 5′ UTR from *ALD6* (P_{ALD6}) and the 3′ UTR and terminator sequence from *SED1* (T_{SED1}). P_{ALD6} was chosen because the *ALD6* mRNA is expressed at similar levels to *SED1* and is not altered in response to CR treatment (Table S2). The resulting construct was chromosomally integrated, and mRNA expression was assessed by qRT-PCR. The T_{SED1} reporter mRNA showed a marked reduction in expression in the absence of Nab6 (*Δnab6*), which could be rescued by additionally deleting *MRN1* (*Δmrn1 Δnab6*) (Figure 5D, top). These data support the model that Nab6 and Mrn1 have opposing effects on *SED1* mRNA abundance, acting posttranscriptionally via the 3′ UTR.

For comparison, we generated a second reporter construct consisting of the promoter and 5′ UTR from *SED1* (P_{SED1}) fused to the Venus CDS and the 3′ UTR and terminator sequence from *ADH1* (T_{ADH1}), which is not stress responsive. This construct is expected to be under transcriptional control of CWI while avoiding Nab6/Mrn1 posttranscriptional regulation. CR treatment induced a robust increase in expression that was abrogated by deletion of *SLT2* (Figure 5D, bottom), confirming that the authentic transcriptional regulation has been recapitulated. By contrast, induction was not affected by loss of Nab6 or Mrn1, consistent with these proteins acting posttranscriptionally.

To confirm that Nab6 and Mrn1 directly impact the stability of target RNAs, we treated cells with the transcription inhibitor thiolutin and followed *SED1* mRNA abundance using qRT-PCR. As expected, *SED1* mRNA was destabilized in the *Δnab6* strain compared with wild type, and the additional deletion of *MRN1* partially reversed this phenotype (Figure 5E). Conversely, the control *RPL6B* mRNA was unperturbed by deletion of Nab6 or Mrn1 (Figure 5F).

DISCUSSION

An estimated ~180 genes are directly involved in cell wall biosynthesis, remodeling, or structure.[30] Many encode proteins that are directly incorporated into the cell wall, but most regulate upstream processing events, such as precursor synthesis, O-mannosylation, N-glycosylation, or GPI attachment. Our CRAC experiments revealed that Mrn1 and Nab6 predominantly target mRNAs from the former group; examples include both structural components of the wall (e.g., *HSP150* and *SED1*) and remodeling enzymes (e.g., *SCW4*, *BGL2*, *DSE2*, and *CTS1*). Typically, these transcripts were bound by Mrn1/Nab6 at only one or two sites within their 3′ UTRs, indicating highly specific binding.

Both Mrn1 and Nab6 also targeted additional mRNAs not directly implicated in cell wall biosynthesis. These included several mRNAs encoding plasma membrane proteins (Pmp1, Pma1, Mrh1, and Nce102) and the mating pheromone Mfa1. These proteins are matured through the same general secretory pathway as cell wall proteins[31–35] (reviewed in Feyder et al.[36] and Free[37]), possibly explaining why seemingly unrelated mRNAs might be regulated by the same RBPs.

One of the most enriched Mrn1-specific targets was the *MRN1* transcript itself (Table S1), suggesting possible autoregulation. Notably, Mrn1 binding to *MRN1* was situated entirely within the 5′ UTR, a pattern contrary to all other major targets (Figure S2C). We speculate that binding to the *MRN1* 5′ UTR might reduce stability and/or inhibit translation, leading to autoregulation.

Most Nab6 targets showed decreased expression in the *Δnab6* strain, and even more so in *Δnab6 Δslt2*, suggesting that Nab6 stabilizes its target mRNAs. The expression changes were relatively modest but phenotypically significant. In the absence of the CWI pathway, Nab6 was completely essential for cells to survive even low levels of CR or CFW. Even in the absence of specific cell wall stress, the *Δnab6 Δslt2* strain was slow growing, suggesting that Nab6 also plays a role in normal CWI and/or the remodeling needed for cell division.

In RNA-seq, four transcripts showed significantly increased expression in the absence of Mrn1, and one of these (*RAD51*) was also a direct mRNA binding target for Mrn1. Another Mrn1 target, *BGL2*, was more modestly increased in *Δmrn1* strains. These results are broadly consistent with a recent study

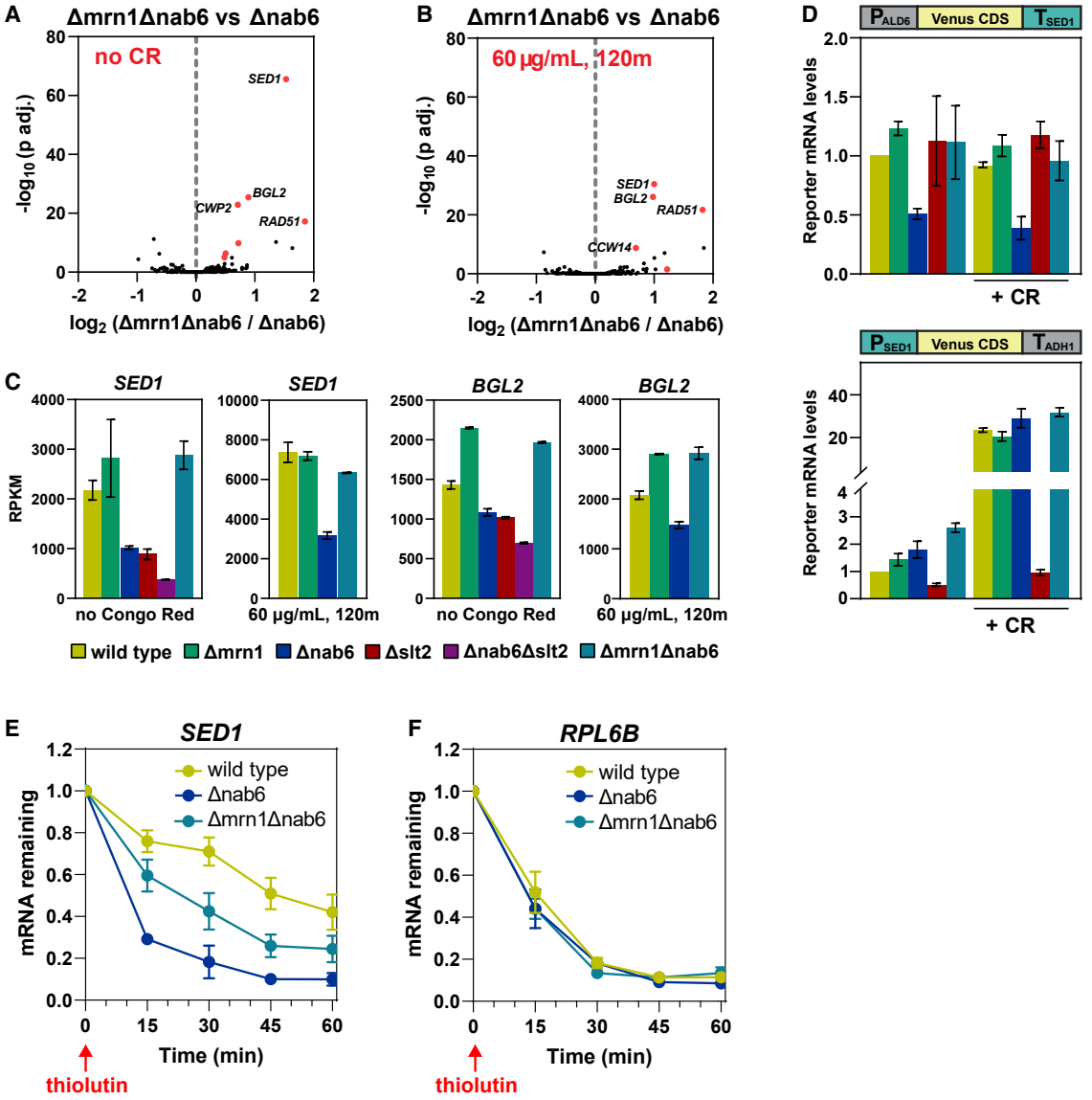

Figure 5. Loss of Mrn1 partially suppresses the phenotype from loss of Nab6

(A and B) Volcano plots showing differentially expressed genes between *Δmrn1 Δnab6* knockout strains and the *Δnab6* single mutant. Transcripts that are significantly altered (p adj. < 0.01) and also a CRAC target of either Mrn1 or Nab6 are colored red. Adjusted p values were calculated using DESeq2.

(C) Bar graphs showing the number of reads (fragments per kilobase per million mapped reads) in each library that map to the *SED1* or *BGL2* transcripts in the absence or presence of CR. Error bars show standard deviation of the mean (n = 2).

(D) Bar graphs showing the mRNA levels for the T_{SED1} (top) and P_{SED1} (bottom) reporter constructs. Error bars show standard deviation of the mean (n = 2). Bar colors are the same as in (C).

(E and F) The transcription inhibitor thiolutin was added to exponentially growing cells, and relative mRNA expression was measured by qRT-PCR. The 25S rRNA was used as a loading control. Error bars show standard error of the mean (n = 3).

analyzing the transcriptome of *Δmrn1* cells[38] that concluded that Mrn1 recruits the cellular RNA degradation machinery. This agrees with our observation that at least some Mrn1 targets are upregulated in the *Δmrn1* strain. However, we cannot exclude the possibility that Mrn1 also regulates additional aspects of gene expression, such as mRNA localization or translation.

An interesting phenotype emerged when we compared the *Δnab6* strain with *Δmrn1 Δnab6* double mutants. *SED1* and *BGL2* were downregulated in the absence of Nab6, but mRNA levels were rescued when Mrn1 was also deleted. Both transcripts were bound by Nab6 and Mrn1 at overlapping sites, supporting a model in which the two proteins compete for binding. In the absence of Nab6, binding of Mrn1 may be enhanced,

destabilizing the mRNA; if both proteins are absent, then "default" mRNA expression is restored. We were initially surprised that Mrn1 and Nab6 have antagonistic functions, at least on some cell wall-related substrates. However, the cell wall must constantly be remodeled to allow for expansion during growth, while retaining integrity against turgor pressure, even in the absence of specific damage. So, an accurate balance between activities that weaken and strengthen the cell wall must always be maintained. We speculate that an interplay between Nab6 and Mrn1 activities aids this process. Notably, Mrn1 binding to mRNAs is also antagonized by another mRNA-binding protein, Pub1,[38] to which it shows a lower degree of homology.

Previous studies of cell wall stress have largely focused on the CWI signaling pathway. In response to cell wall damage, the CWI pathway broadly activates the transcription of cell wall-related mRNAs. Phenotypic changes induced by transcriptional regulation are generally strong but also relatively slow; induced mRNAs must be transcribed, processed, and exported prior to translation. Posttranscriptional regulation bypasses some or all of these steps, potentially eliciting a much faster response. Posttranscriptional control also allows fine-tuning; mRNAs can be localized and translated only when and where they are needed, e.g., at sites of cell wall growth or repair. Ssd1 appears to function precisely in this way, repressing translation of mRNAs until they are delivered to the bud neck.[17] Nab6 may have an analogous role, stabilizing and/or activating translation of mRNAs destined for sites of growth or repair.

Recent work from the Chanfreau lab highlighted the importance of posttranscriptional regulation for cell wall homeostasis.[39] The *Δslt2* strain is severely impaired in response to heat shock, a condition that also induces cell wall stress.[39,40] However, additional deletion of various individual mRNA decay factors (e.g., the exosome, Xrn1, or Upf1) was sufficient to restore growth.[39] This observation suggests that RNA synthesis and degradation are in balance. To survive cell wall stress, cells must either transcribe new cell wall mRNAs or stabilize the existing pool. By protecting its target mRNAs, Nab6 may partially compensate for the absence of transcriptional regulation in *Δslt2* cells. Only in the absence of both Slt2 and Nab6 do cells become especially vulnerable to cell wall damage.

Limitations of the study

Our results implicate Nab6 and Mrn1 as regulators of cell wall homeostasis, but major mechanistic questions remain unresolved. Most importantly, how does Nab6 stabilize its target mRNAs? Is this its only function, or does Nab6 also regulate mRNA localization and/or translation? More broadly, why do so many RBPs specifically target cell wall mRNAs,[15,16,41] and do they act independently or in concert? The cell wall is an important target for several clinically approved antifungal agents, but their use is limited by fungal resistance.[42–44] Identifying the mechanisms by which fungi respond to cell wall stress will ultimately result in improved treatment options.

STAR★METHODS

Detailed methods are provided in the online version of this paper and include the following:

SUPPLEMENTAL INFORMATION

Supplemental information can be found online at https://doi.org/10.1016/j.celrep.2023.112184.

ACKNOWLEDGMENTS

We thank Richard Clark, Audrey Coutts, and Angie Fawkes from the Edinburgh Wellcome Clinical Research Facility for sequencing services, as well as Shaun Webb from the WCB bioinformatics core facility for maintaining the servers we used for processing sequencing data. This work was funded by Wellcome Principal Research Fellowships to D.T. (109916 and 222516), also supporting S.B. and V.S., and core funding for the Wellcome Center for Cell Biology (203149).

AUTHOR CONTRIBUTIONS

Conceptualization, S.B., V.S., and D.T.; experiments, S.B. and V.S.; data analysis, S.B.; writing – original draft, S.B.; writing – review & editing, S.B., D.T., and V.S.; funding acquisition, D.T.

DECLARATION OF INTERESTS

The authors declare no competing interests.

Received: September 30, 2022
Revised: January 5, 2023
Accepted: February 14, 2023

REFERENCES

1. Gow, N.A.R., Latge, J.P., and Munro, C.A. (2017). The fungal cell wall: structure, biosynthesis, and function. Microbiol. Spectr. *5*. https://doi.org/10.1128/microbiolspec.FUNK-0035-2016.
2. Szymański, M., Chmielewska, S., Czyżewska, U., Malinowska, M., and Tylicki, A. (2022). Echinocandins - structure, mechanism of action and use in antifungal therapy. J. Enzyme Inhib. Med. Chem. *37*, 876–894. https://doi.org/10.1080/14756366.2022.2050224.
3. Roncero, C., and Durán, A. (1985). Effect of Calcofluor white and Congo red on fungal cell wall morphogenesis: in vivo activation of chitin polymerization. J. Bacteriol. *163*, 1180–1185. https://doi.org/10.1128/jb.163.3.1180-1185.1985.

4. Elorza, M.V., Rico, H., and Sentandreu, R. (1983). Calcofluor white alters the assembly of chitin fibrils in Saccharomyces cerevisiae and Candida albicans cells. J. Gen. Microbiol. *129*, 1577–1582. https://doi.org/10.1099/00221287-129-5-1577.

5. Sanz, A.B., García, R., Pavón-Vergés, M., Rodríguez-Peña, J.M., and Arroyo, J. (2022). Control of gene expression via the yeast CWI pathway. Int. J. Mol. Sci. *23*, 1791. https://doi.org/10.3390/ijms23031791.

6. García, R., Bermejo, C., Grau, C., Pérez, R., Rodríguez-Peña, J.M., Francois, J., Nombela, C., and Arroyo, J. (2004). The global transcriptional response to transient cell wall damage in Saccharomyces cerevisiae and its regulation by the cell integrity signaling pathway. J. Biol. Chem. *279*, 15183–15195. https://doi.org/10.1074/jbc.M312954200.

7. Sanz, A.B., García, R., Rodríguez-Peña, J.M., Díez-Muñiz, S., Nombela, C., Peterson, C.L., and Arroyo, J. (2012). Chromatin remodeling by the SWI/SNF complex is essential for transcription mediated by the yeast cell wall integrity MAPK pathway. Mol. Biol. Cell *23*, 2805–2817. https://doi.org/10.1091/mbc.E12-04-0278.

8. Yurko, N., Liu, X., Yamazaki, T., Hoque, M., Tian, B., and Manley, J.L. (2017). MPK1/SLT2 links multiple stress responses with gene expression in budding yeast by phosphorylating Tyr1 of the RNAP II CTD. Mol. Cell *68*, 913–925.e3. https://doi.org/10.1016/j.molcel.2017.11.020.

9. Stieg, D.C., Willis, S.D., Ganesan, V., Ong, K.L., Scuorzo, J., Song, M., Grose, J., Strich, R., and Cooper, K.F. (2018). A complex molecular switch directs stress-induced cyclin C nuclear release through SCF(Grr1)-mediated degradation of Med13. Mol. Biol. Cell *29*, 363–375. https://doi.org/10.1091/mbc.E17-08-0493.

10. Jin, C., Strich, R., and Cooper, K.F. (2014). Slt2p phosphorylation induces cyclin C nuclear-to-cytoplasmic translocation in response to oxidative stress. Mol. Biol. Cell *25*, 1396–1407. https://doi.org/10.1091/mbc.E13-09-0550.

11. Krasley, E., Cooper, K.F., Mallory, M.J., Dunbrack, R., and Strich, R. (2006). Regulation of the oxidative stress response through Slt2p-dependent destruction of cyclin C in Saccharomyces cerevisiae. Genetics *172*, 1477–1486. https://doi.org/10.1534/genetics.105.052266.

12. García, R., Botet, J., Rodríguez-Peña, J.M., Bermejo, C., Ribas, J.C., Revuelta, J.L., Nombela, C., and Arroyo, J. (2015). Genomic profiling of fungal cell wall-interfering compounds: identification of a common gene signature. BMC Genom. *16*, 683. https://doi.org/10.1186/s12864-015-1879-4.

13. Bermejo, C., Rodríguez, E., García, R., Rodríguez-Peña, J.M., Rodríguez de la Concepción, M.L., Rivas, C., Arias, P., Nombela, C., Posas, F., and Arroyo, J. (2008). The sequential activation of the yeast HOG and SLT2 pathways is required for cell survival to cell wall stress. Mol. Biol. Cell *19*, 1113–1124. https://doi.org/10.1091/mbc.E07-08-0742.

14. Hall, R.A., and Wallace, E.W.J. (2022). Post-transcriptional control of fungal cell wall synthesis. Cell Surf. *8*, 100074. https://doi.org/10.1016/j.tcsw.2022.100074.

15. Hogan, D.J., Riordan, D.P., Gerber, A.P., Herschlag, D., and Brown, P.O. (2008). Diverse RNA-binding proteins interact with functionally related sets of RNAs, suggesting an extensive regulatory system. PLoS Biol. *6*, e255. https://doi.org/10.1371/journal.pbio.0060255.

16. Bayne, R.A., Jayachandran, U., Kasprowicz, A., Bresson, S., Tollervey, D., Wallace, E.W.J., and Cook, A.G. (2022). Yeast Ssd1 is a non-enzymatic member of the RNase II family with an alternative RNA recognition site. Nucleic Acids Res. *50*, 2923–2937. https://doi.org/10.1093/nar/gkab615.

17. Jansen, J.M., Wanless, A.G., Seidel, C.W., and Weiss, E.L. (2009). Cbk1 regulation of the RNA-binding protein Ssd1 integrates cell fate with translational control. Curr. Biol. *19*, 2114–2120. https://doi.org/10.1016/j.cub.2009.10.071.

18. Hu, Z., Xia, B., Postnikoff, S.D., Shen, Z.J., Tomoiaga, A.S., Harkness, T.A., Seol, J.H., Li, W., Chen, K., and Tyler, J.K. (2018). Ssd1 and Gcn2 suppress global translation efficiency in replicatively aged yeast while their activation extends lifespan. Elife *7*, e35551. https://doi.org/10.7554/eLife.35551.

19. Lee, A.Y., St Onge, R.P., Proctor, M.J., Wallace, I.M., Nile, A.H., Spagnuolo, P.A., Jitkova, Y., Gronda, M., Wu, Y., Kim, M.K., et al. (2014). Mapping the cellular response to small molecules using chemogenomic fitness signatures. Science *344*, 208–211. https://doi.org/10.1126/science.1250217.

20. Costanzo, M., VanderSluis, B., Koch, E.N., Baryshnikova, A., Pons, C., Tan, G., Wang, W., Usaj, M., Hanchard, J., Lee, S.D., et al. (2016). A global genetic interaction network maps a wiring diagram of cellular function. Science *353*, aaf1420. https://doi.org/10.1126/science.aaf1420.

21. Bresson, S., Shchepachev, V., Spanos, C., Turowski, T.W., Rappsilber, J., and Tollervey, D. (2020). Stress-induced translation inhibition through rapid displacement of scanning initiation factors. Mol. Cell *80*, 470–484.e8. https://doi.org/10.1016/j.molcel.2020.09.021.

22. Shchepachev, V., Bresson, S., Spanos, C., Petfalski, E., Fischer, L., Rappsilber, J., and Tollervey, D. (2019). Defining the RNA interactome by total RNA-associated protein purification. Mol. Syst. Biol. *15*, e8689. https://doi.org/10.15252/msb.20188689.

23. Jumper, J., Evans, R., Pritzel, A., Green, T., Figurnov, M., Ronneberger, O., Tunyasuvunakool, K., Bates, R., Žídek, A., Potapenko, A., et al. (2021). Highly accurate protein structure prediction with AlphaFold. Nature *596*, 583–589. https://doi.org/10.1038/s41586-021-03819-2.

24. Varadi, M., Anyango, S., Deshpande, M., Nair, S., Natassia, C., Yordanova, G., Yuan, D., Stroe, O., Wood, G., Laydon, A., et al. (2022). AlphaFold Protein Structure Database: massively expanding the structural coverage of protein-sequence space with high-accuracy models. Nucleic Acids Res. *50*, D439–D444. https://doi.org/10.1093/nar/gkab1061.

25. Granneman, S., Kudla, G., Petfalski, E., and Tollervey, D. (2009). Identification of protein binding sites on U3 snoRNA and pre-rRNA by UV cross-linking and high-throughput analysis of cDNAs. Proc. Natl. Acad. Sci. USA *106*, 9613–9618. https://doi.org/10.1073/pnas.0901997106.

26. Chin, B.L., Ryan, O., Lewitter, F., Boone, C., and Fink, G.R. (2012). Genetic variation in Saccharomyces cerevisiae: circuit diversification in a signal transduction network. Genetics *192*, 1523–1532. https://doi.org/10.1534/genetics.112.145573.

27. Laz, E.V., Lee, J., and Levin, D.E. (2020). Crosstalk between Saccharomycescerevisiae SAPKs Hog1 and Mpk1 is mediated by glycerol accumulation. Fungal Biol. *124*, 361–367. https://doi.org/10.1016/j.funbio.2019.10.002.

28. Shimoi, H., Kitagaki, H., Ohmori, H., Iimura, Y., and Ito, K. (1998). Sed1p is a major cell wall protein of Saccharomyces cerevisiae in the stationary phase and is involved in lytic enzyme resistance. J. Bacteriol. *180*, 3381–3387. https://doi.org/10.1128/JB.180.13.3381-3387.1998.

29. Boorsma, A., de Nobel, H., ter Riet, B., Bargmann, B., Brul, S., Hellingwerf, K.J., and Klis, F.M. (2004). Characterization of the transcriptional response to cell wall stress in Saccharomyces cerevisiae. Yeast *21*, 413–427. https://doi.org/10.1002/yea.1109.

30. Orlean, P. (2012). Architecture and biosynthesis of the Saccharomyces cerevisiae cell wall. Genetics *192*, 775–818. https://doi.org/10.1534/genetics.112.144485.

31. Michaelis, S., and Barrowman, J. (2012). Biogenesis of the Saccharomyces cerevisiae pheromone a-factor, from yeast mating to human disease. Microbiol. Mol. Biol. Rev. *76*, 626–651. https://doi.org/10.1128/MMBR.00010-12.

32. Luo, W.j., and Chang, A. (2000). An endosome-to-plasma membrane pathway involved in trafficking of a mutant plasma membrane ATPase in yeast. Mol. Biol. Cell *11*, 579–592. https://doi.org/10.1091/mbc.11.2.579.

33. Grossmann, G., Malinsky, J., Stahlschmidt, W., Loibl, M., Weig-Meckl, I., Frommer, W.B., Opekarová, M., and Tanner, W. (2008). Plasma membrane microdomains regulate turnover of transport proteins in yeast. J. Cell Biol. *183*, 1075–1088. https://doi.org/10.1083/jcb.200806035.

34. Coïc, Y.M., Vincent, M., Gallay, J., Baleux, F., Mousson, F., Beswick, V., Neumann, J.M., and de Foresta, B. (2005). Single-spanning membrane protein insertion in membrane mimetic systems: role and localization of

aromatic residues. Eur. Biophys. J. *35*, 27–39. https://doi.org/10.1007/s00249-005-0002-1.

35. Wu, K., Dawe, J.H., and Aris, J.P. (2000). Expression and subcellular localization of a membrane protein related to Hsp30p in Saccharomyces cerevisiae. Biochim. Biophys. Acta *1463*, 477–482. https://doi.org/10.1016/s0005-2736(99)00255-2.
36. Feyder, S., De Craene, J.O., Bär, S., Bertazzi, D.L., and Friant, S. (2015). Membrane trafficking in the yeast Saccharomyces cerevisiae model. Int. J. Mol. Sci. *16*, 1509–1525. https://doi.org/10.3390/ijms16011509.
37. Free, S.J. (2013). Fungal cell wall organization and biosynthesis. Adv. Genet. *81*, 33–82. https://doi.org/10.1016/b978-0-12-407677-8.00002-6.
38. Reynaud, K., Brothers, M., Ly, M., and Ingolia, N.T. (2021). Dynamic post-transcriptional regulation by Mrn1 links cell wall homeostasis to mitochondrial structure and function. PLoS Genet. *17*, e1009521. https://doi.org/10.1371/journal.pgen.1009521.
39. Wang, C., Liu, Y., DeMario, S.M., Mandric, I., Gonzalez-Figueroa, C., and Chanfreau, G.F. (2020). Rrp6 moonlights in an RNA exosome-independent manner to promote cell survival and gene expression during stress. Cell Rep. *31*, 107754. https://doi.org/10.1016/j.celrep.2020.107754.
40. de Nobel, H., Ruiz, C., Martin, H., Morris, W., Brul, S., Molina, M., and Klis, F.M. (2000). Cell wall perturbation in yeast results in dual phosphorylation of the Slt2/Mpk1 MAP kinase and in an Slt2-mediated increase in FKS2-lacZ expression, glucanase resistance and thermotolerance. Microbiology (Read.) *146*, 2121–2132. https://doi.org/10.1099/00221287-146-9-2121.
41. Tuck, A.C., and Tollervey, D. (2013). A transcriptome-wide atlas of RNP composition reveals diverse classes of mRNAs and lncRNAs. Cell *154*, 996–1009. https://doi.org/10.1016/j.cell.2013.07.047.
42. Wagener, J., and Loiko, V. (2017). Recent insights into the paradoxical effect of echinocandins. J. Fungi *4*, 5. https://doi.org/10.3390/jof4010005.
43. Chandrasekar, P.H. (2007). Increased dose of echinocandins for invasive fungal infections: bonanza for the patient or the pharmaceutical industry? Bone Marrow Transplant. *39*, 129–131. https://doi.org/10.1038/sj.bmt.1705563.
44. Eschenauer, G., Depestel, D.D., and Carver, P.L. (2007). Comparison of echinocandin antifungals. Ther. Clin. Risk Manag. *3*, 71–97. https://doi.org/10.2147/tcrm.2007.3.1.71.
45. Dobin, A., Davis, C.A., Schlesinger, F., Drenkow, J., Zaleski, C., Jha, S., Batut, P., Chaisson, M., and Gingeras, T.R. (2013). STAR: ultrafast universal RNA-seq aligner. Bioinformatics *29*, 15–21. https://doi.org/10.1093/bioinformatics/bts635.
46. Robinson, J.T., Thorvaldsdóttir, H., Winckler, W., Guttman, M., Lander, E.S., Getz, G., and Mesirov, J.P. (2011). Integrative genomics viewer. Nat. Biotechnol. *29*, 24–26. https://doi.org/10.1038/nbt.1754.
47. Webb, S., Hector, R.D., Kudla, G., and Granneman, S. (2014). PAR-CLIP data indicate that Nrd1-Nab3-dependent transcription termination regulates expression of hundreds of protein coding genes in yeast. Genome Biol. *15*, R8. https://doi.org/10.1186/gb-2014-15-1-r8.
48. Quinlan, A.R., and Hall, I.M. (2010). BEDTools: a flexible suite of utilities for comparing genomic features. Bioinformatics *26*, 841–842. https://doi.org/10.1093/bioinformatics/btq033.
49. Dodt, M., Roehr, J.T., Ahmed, R., and Dieterich, C. (2012). Flexbar-flexible barcode and adapter processing for next-generation sequencing platforms. Biology *1*, 895–905. https://doi.org/10.3390/biology1030895.
50. Eden, E., Navon, R., Steinfeld, I., Lipson, D., and Yakhini, Z. (2009). GOrilla: a tool for discovery and visualization of enriched GO terms in ranked gene lists. BMC Bioinf. *10*, 48. https://doi.org/10.1186/1471-2105-10-48.
51. Liebermeister, W., Noor, E., Flamholz, A., Davidi, D., Bernhardt, J., and Milo, R. (2014). Visual account of protein investment in cellular functions. Proc. Natl. Acad. Sci. USA *111*, 8488–8493. https://doi.org/10.1073/pnas.1314810111.
52. Liao, Y., Smyth, G.K., and Shi, W. (2014). featureCounts: an efficient general purpose program for assigning sequence reads to genomic features. Bioinformatics *30*, 923–930. https://doi.org/10.1093/bioinformatics/btt656.
53. Love, M.I., Huber, W., and Anders, S. (2014). Moderated estimation of fold change and dispersion for RNA-seq data with DESeq2. Genome Biol. *15*, 550. https://doi.org/10.1186/s13059-014-0550-8.
54. Laughery, M.F., Hunter, T., Brown, A., Hoopes, J., Ostbye, T., Shumaker, T., and Wyrick, J.J. (2015). New vectors for simple and streamlined CRISPR-Cas9 genome editing in Saccharomyces cerevisiae. Yeast *32*, 711–720. https://doi.org/10.1002/yea.3098.
55. Lee, M.E., DeLoache, W.C., Cervantes, B., and Dueber, J.E. (2015). A highly characterized yeast toolkit for modular, multipart assembly. ACS Synth. Biol. *4*, 975–986. https://doi.org/10.1021/sb500366v.

STAR★METHODS

KEY RESOURCES TABLE

REAGENT or RESOURCE	SOURCE	IDENTIFIER
Chemicals, peptides, and recombinant proteins		
Synthetic dropout (SD) -trp -met	Formedium	Cat#DCS0641
Yeast nitrogen base	Formedium	Cat#CYN0405
Congo Red	Sigma-Aldrich	Cat#C6767
Calcofluor White	Sigma-Aldrich	Cat#F3543
Caspofungin	Stratech	Cat#B4972
Thiolutin	Cayman	Cat#11350
SwaI	NEB	Cat#R0604S
BclI-HF	NEB	Cat#R3160S
T4 DNA ligase buffer	NEB	Cat#B020S
T4 DNA ligase	NEB	Cat#M0202L
dNTPs	Takara	Cat#RR002M
Klenow exo-	NEB	Cat#M0212L
Protease-inhibitor cocktail	Roche	Cat#11873580001
Magnetic anti-Flag bead slurry	Sigma-Aldrich	Cat#M8823; RRID: AB_2637089
Flag peptide	Sigma-Aldrich	Cat#F3290
RNace-IT	Agilent	Cat#400720
TSAP	Promega	Cat#M9910
RNaseIN	Promega	Cat#N2511
T4 RNA ligase I	NEB	Cat#M0204L
T4 RNA ligase II truncated K227Q	NEB	Cat#M0351L
T4 PNK	NEB	Cat#M0201L
NuPAGE sample loading buffer	Invitrogen	Cat#NP0007
NuPAGE MOPS buffer	Invitrogen	Cat#NP001-02
NuPAGE transfer buffer	Invitrogen	Cat#NP0006-1
Proteinase K	Roche	Cat#03115836001
Superscript III	Invitrogen	Cat#18080-044
La Taq	Takara	Cat#RR002M
Metaphore agarose	Lonza	Cat#50180
Glycoblue	Fisher Scientific	Cat#AM9516
T4 DNA ligase	NEB	Cat#M020S
BsaI-HFv2	NEB	Cat#R3733S
NotI-HF	NEB	Cat#R3189S
hygromycin	Millipore	Cat#400052-50ML
Turbo DNase	Thermo Fisher	Cat#AM2238
Critical commercial assays		
Nickel beads	Qiagen	Cat#30410
Spin-columns	Thermo Scientific	Cat#69725
4-12% Bis-Tris NuPAGE gel	Invitrogen	Cat#NP0321BOX
Hybond-N+ nitrocellulose membranes	GE Healthcare	Cat#RPN303B
DNA gel extraction kit	Qiagen	Cat#28606
Zirconia beads	Thistle Scientific	Cat#ZrOB05
Poly(A) mRNA magnetic isolation kit	NEB	Cat#E7490
NEBNEXT Ultra II Directional RNA Library Prep kit	NEB	Cat#7760
Luna Universal one-step RT-qPCR kit	NEB	Cat#E3005S

(*Continued on next page*)

Continued

REAGENT or RESOURCE	SOURCE	IDENTIFIER
Deposited data		
CRAC and RNA-seq raw data	NCBI gene expression omnibus	Gene Expression Omnibus: GSE210558
Experimental models: Organisms/strains		
Saccharomyces cerevisiae BY4741 ('wild type') strain	Euroscarf	ySB001
For strains generated in this study, see Table S5.	This study	N/A
Oligonucleotides		
See Table S6.	This study	N/A
Recombinant DNA		
See Table S4.	This study	N/A
Software and algorithms		
Novoalign v2.07.00	Novocraft	http://www.novocraft.com/products/novoalign/
STAR 2.7.5a	Dobin et al.[45]	N/A
Integrated Genomics Viewer	Robinson et al.[46]	http://software.broadinstitute.org/software/igv/
Prism 9	GraphPad	https://www.graphpad.com/
pyCRAC	Webb et al.[47]	http://sandergranneman.bio.ed.ac.uk/pycrac-software
Bedtools v2.27.0	Quinlan and Hall[48]	https://github.com/arq5x/bedtools2
Flexbar v3.4.0	Dodt et al.[49]	https://github.com/seqan/flexbar
GOrilla	Eden et al.[50]	http://cbl-gorilla.cs.technion.ac.il/
BBduk	Department of Energy-Joint Genome Institute	https://sourceforge.net/projects/bbmap
Proteomaps	Liebermeister et al.[51]	https://www.proteomaps.net/
featureCounts	Liao et al.[52]	https://subread.sourceforge.net/
PyMOL	N/A	https://pymol.org/2/
Morpheus	Broad Institute	https://software.broadinstitute.org/morpheus/
DESeq2	Love et al.[53]	https://bioconductor.org/packages/release/bioc/html/DESeq2.html
ggplot2	N/A	https://cran.r-project.org/web/packages/ggplot2/index.html

RESOURCE AVAILABILITY

Lead contact

Further information and requests for resources and reagents should be directed to the lead contact, David Tollervey (d.tollervey@ed.ac.uk).

Materials availability

Plasmids and strains generated in this study are available from the lead contact upon request.

Data and code availability

- CRAC and RNA-seq datasets have been deposited at GEO and are publicly available as of the date of publication. Accession numbers are listed in the key resources table.
- This paper does not report original code.
- Any additional information required to reanalyze the data reported in this paper is available from the lead contact upon request.

EXPERIMENTAL MODEL AND SUBJECT DETAILS

All S. cerevisiae strains used in this study were derived from the BY4741 background (*MATa his3Δ1 leu2Δ0 met15Δ0 ura3Δ0*).

METHOD DETAILS

Cell culture and medium

All yeast strains were cultured at 30°C in synthetic dropout (SD) -trp -met (Formedium Cat#DCS0641) supplemented with 20 μg/mL methionine, yeast nitrogen base (Formedium Cat#CYN0405), and 2% glucose. CRAC samples were crosslinked at 0.4 OD_{600}. Growth curves and RNAseq experiments were initiated at 0.125 OD_{600} with varying concentrations of Congo Red (Sigma-Aldrich Cat#C6767) or Calcofluor White (Sigma-Aldrich Cat#F3543). For the 10-fold serial dilution assays, cells were grown to stationary phase overnight, diluted to 0.5 OD_{600}, and spotted on -trp plates supplemented with varying concentrations of Congo Red or caspofungin (Stratech Cat#B4972). For transcription inhibition experiments, cells were grown to 0.7 OD_{600} and treated with 6 μg/mL thiolutin (Cayman Cat#11350).

Gene tagging and deletion

For CRAC experiments, the chromosomal copies of MRN1 and NAB6 were C-terminally tagged with HF (His-Flag), consisting of eight consecutive histidine residues, a four alanine spacer, and a single Flag motif (HHHHHHHHAAAADYKDDDDK). The two proteins were tagged using CRISPR-Cas9 and the pML104 vector[54] as described below.

The pML104 vector included a Cas9 expression construct, a URA3 selectable marker, and a guide RNA (gRNA) cloning site. Approximately 10 μg of plasmid was digested overnight with SwaI (NEB Cat#R0604S), and then for 2 h at 50°C with BclI-HF (NEB Cat#R3160S). The digested vector was purified by gel extraction, and aliquoted for later use.

Guide RNA oligos were designed as previously reported.[54] Each oligo pair was annealed in a reaction consisting of 1 μM forward oligo, 1 μM reverse oligo, and 1X T4 DNA ligase buffer (NEB Cat#B020S) in a 100 μL reaction volume. The hybridization reaction was initially incubated at 95°C for 6 min, and gradually decreased to 25°C at the rate of 1.33 °C/min. Hybridized substrates were then ligated into the digested vector at 25°C for 4 h. The ligation reaction consisted of 265 ng pre-cut pML104 vector, 0.8 nmol insert, 1X T4 DNA ligase buffer, and 800U of T4 DNA ligase (NEB Cat#M0202L) in a 40 μL reaction volume. The ligation mix was transformed into homemade DH5a E. coli, and plated overnight on LB-Amp. Plasmid DNA was isolated and sequenced to ensure correct insertion of the guide sequence.

To insert the HF tag, we designed fragments consisting of the HF DNA sequence flanked by 50 bp homology arms to serve as repair templates. Synonymous mutations were typically incorporated into each construct in order to disrupt the PAM site and prevent further cleavage by Cas9. Each repair template was made by annealing two single-stranded oligonucleotides sharing 20 bp of complementarity at their 3′ ends. Each set of oligos was annealed in a reaction consisting of 10 μM forward oligo, 10 μM reverse oligo, and 1X NEB buffer 2.1 in a 43 μL reaction volume. The hybridization reaction was initially incubated at 95°C for 6 min, and gradually decreased to 25 °C at the rate of 1.33°C/min. Subsequently, the annealed oligos were incubated in the same buffer supplemented with 250 μM dNTPs (Takara Cat#RR002M) and 5U Klenow exo- (NEB Cat#M0212L) in a 50 μL reaction at 37°C for 1 h to fill in the single-stranded regions. To introduce the HF tag, BY4741 yeast were transformed using the standard PEG/LiOAc protocol with 500 ng of gRNA plasmid and 10 pmol of the corresponding repair template. Transformants were plated onto -ura medium. After three days, several clones from each transformation were plated again on selective medium, and allowed to grow for an additional 2–3 days. Single colonies were selected and plated on YPD for 2 days. Finally, individual colonies were grown overnight in liquid YPD and frozen. The clones were verified by PCR using flanking primers and confirmed by sequencing.

All gene deletions were made using CRISPR/Cas9, essentially as described above, with the exception of *HOG1* and *SED1*. The *Δhog1* strain was generated with conventional homologous replacement using a *HIS3* selectable marker derived from pFA6a-HIS3MX6 (Addgene: 41596). The *Δsed1* strain was acquired from the Euroscarf haploid deletion collection for BY4741.

CRAC

The CRAC protocol was performed as previously described.[21] For each CRAC experiment, 700 mL of cells were cultured in SD -trp medium. At OD_{600} 0.4 the cells were UV-irradiated at 254 nm with a dose of 100 mJ/cm^2 (4–6 s) using the Vari-X-Link crosslinker. Following crosslinking, cells were collected by filtration and resuspended in 50 mL of ice-cold PBS, and centrifuged at 4600g for 2 min. The cell pellets were frozen and stored at −80°C. Subsequently, cell pellets were resuspended in 500 μL TN150 (50 mM Tris-HCl pH 7.5, 150 mM NaCl, 0.1% NP-40, 5 mM β-mercaptoethanol and a protease-inhibitor cocktail (1 tablet/50 mL) (Roche Cat#11873580001). The resuspended cells were added to 1.25 mL zirconia beads in a 50 mL conical and lysed using 5 1-min pulses, with cooling on ice in between. The resulting lysate was further diluted with 1.5 mL TN150, briefly vortexed, and centrifuged at 4600g for 5 min. The supernatant was transferred to a 1.5 mL Eppendorf tube and centrifuged at 16000g for 20 min. In parallel, 100 μL of magnetic anti-Flag bead slurry (Sigma-Aldrich Cat#M8823) was washed twice with TN150. The cleared lysate was incubated with the anti-Flag beads at 4°C with nutating. After 2 h, the supernatant was removed, and the beads were washed four times with TN150 (5 min nutating at 4°C for each wash). To elute the protein of interest, the beads were incubated with 20 μg of Flag peptide (Sigma-Aldrich Cat#F3290) in a 200 μL volume at 37°C for 15 min with shaking. The eluate was transferred to a fresh tube containing 350 μL TN150 and treated with RNace-IT (Agilent Cat#400720) (0.1U, 5 min, 37°C) to fragment RNA. The RNase reaction was halted by transferring the eluate to a tube containing 400 μg guanidine hydrochloride. The solution was adjusted for nickel affinity purification with the addition of 27 μL 5 M NaCl and 3 μL 2.5 M imidazole, and added to 50 μL of washed nickel beads (Qiagen Cat#30410). After overnight nutation at 4°C, the beads were transferred to a spin column (Thermo Scientific Cat#69725), washed 3 times with 400 μL

WBI (6 M guanidine hydrochloride, 50 mM Tris-HCl pH 7.5, 300 mM NaCl, 0.1% NP-40, 10 mM imidazole, and 5 mM β-mercaptoethanol), and then 3 times with 600 μL PNK buffer (50mM Tris-HCl pH 7.5, 10 mM $MgCl_2$, 0.5% NP-40, and 5 mM β-mercaptoethanol). Four subsequent reactions (80 μL each) were performed on-column, and subsequently washed once with WBI and three times with PNK buffer.

1. Phosphatase treatment (1x PNK buffer, 8U TSAP (Promega, Cat#M9910), 80U RNaseIN (Promega Cat#N2511); 37°C for 30 min).
2. 3′ linker ligation (1x PNK buffer, 20U T4 RNA ligase I (NEB Cat#M0204L), 20U T4 RNA ligase II truncated K227Q (NEB Cat#M0351L), 80U RNaseIN, 1 μM Preadenylated 3′ miRcat-33 linker (IDT); 25°C for 6 h).
3. 5′ end phosphorylation and radiolabeling (1x PNK buffer, 40U T4 PNK (NEB Cat#M0201L), 40 μCi ^{32}P-γATP; 37°C for 60 min, with addition of 100 nmol ATP after 40 min).
4. 5′ linker ligation (1x PNK buffer, 40U T4 RNA ligase I, 80U RNaseIN, 5′ linker, 1 mM ATP; 16°C overnight).

After the final ligation reaction, the beads were washed twice with WBII (50 mM Tris-HCl pH 7.5, 50 mM NaCl, 0.1% NP-40, 10 mM imidazole, and 5 mM β-mercaptoethanol). Protein:RNA complexes were eluted twice (10 min each) in 40 μL elution buffer (same as WBII but with 300 mM imidazole). At this point, different replicates for the same protein were combined. The merged eluates were precipitated with 5X volume acetone at −20°C for at least 2 h. Protein:RNA complexes were pelleted (16000g, 20 min, 4°C) and re-suspended in 20 μL 1X NuPAGE sample loading buffer (Invitrogen Cat#NP0007) supplemented with 8% β-mercaptoethanol. The sample was denatured by incubation at 65°C for 10 min and run on a 4–12% Bis-Tris NuPAGE gel (Invitrogen Cat#NP0321BOX) at 150V in 1X NuPAGE MOPS buffer (Invitrogen Cat#NP001-02). The protein:RNA complexes were transferred to Hybond-N+ nitrocellulose membranes (GE Healthcare Cat#RPN303B) with NuPAGE transfer buffer (Invitrogen Cat#NP0006-1) for 1.5 h at 100V, and detected using autoradiography. The appropriate region was excised from the membrane and treated with 0.25 mg/mL Proteinase K (Roche Cat#03115836001) for 2 h at 55°C in a 500 μL reaction consisting of 50 mM Tris-HCl pH 7.5, 50 mM NaCl, 0.1% NP-40, 10 mM imidazole, 1% SDS, 5 mM EDTA, and 5 mM β-mercaptoethanol. The RNA component was isolated using phenol:chloroform extraction followed by ethanol precipitation. Subsequently, the RNA was reverse transcribed using Superscript III (Invitrogen Cat#18080-044) and the miRCat-33 RT oligo (IDT) for 1 h at 50°C in a 20 μL reaction. The resulting cDNA was amplified by PCR in five separate reactions using La Taq (Takara, Cat#RR002M) (2 μL template in each reaction, 21 cycles). The PCR reactions were combined, precipitated in ethanol, and resolved on a 3% Metaphore agarose gel (Lonza Cat#50180). A region corresponding to 140–200 bp was excised from the gel and extracted using a DNA gel extraction kit (QIAGEN Cat#28606). Libraries were sequenced by the Wellcome Trust Clinical Research Facility (Edinburgh, UK) on Next-seq with single-end, 75-nt output.

RNA-seq

Approximately 6 ODs of cells were harvested by centrifugation (4600 rpm; 1min) and frozen at −80°C. Subsequently, the cells were lysed using zirconia beads (Thistle Scientific Cat#ZrOB05) and RNA was extracted with phenol:chloroform followed by ethanol precipitation. Glycoblue (Fisher Scientific Cat#AM9516) was used as a coprecipitant and to visualize the RNA pellet after centrifugation. Libraries for RNAseq were prepared by the Wellcome Trust Clinical Research Facility at Western General Hospital (Edinburgh, UK) using the poly(A) mRNA magnetic isolation kit (NEB Cat#E7490) and the NEBNEXT Ultra II Directional RNA Library Prep kit (NEB Cat#7760), and then sequenced using Next-Seq with paired-end, 100-nt output.

Reporter constructs

The reporter constructs were designed using the modular cloning system devised by the Dueber lab.[55] In this system, each reporter cassette is comprised of nine different 'parts', such as promoters, coding sequence, terminators, etc. A collection of standard parts was obtained from Addgene (Kit# 1000000061), and parts specific to this study were generated using standard PCR and cloning techniques.[55]

Individual parts were combined into reporter cassettes in a reaction consisting of 50 ng of each part plasmid, 1 μL T4 DNA ligase buffer, 0.5 μL T4 DNA ligase (NEB Cat#M020S), 0.5 μL BsaI-HFv2 (NEB Cat#R3733S), and water to bring the final volume to 10 μL. Reaction mixtures were incubated in a thermocycler for 25 cycles of digestion and ligation (42°C for 2 min, 16°C for 5 min) followed by a final digestion step (60°C for 10 min) and heat inactivation (80°C for 10 min). The assembled plasmids were confirmed via diagnostic restriction digest. Subsequently, the plasmids were linearized by digestion with NotI-HF (NEB Cat#R3189S), and transformed into the desired strains. Clones were selected on YPD supplemented with 200 μg/mL hygromycin (Millipore Cat#400052-50ML) and verified by PCR. Reporter experiments were performed in both technical and biological duplicate. The two technical replicates were averaged together to make one biological replicate.

qPCR

Approximately 2 ODs of cells were harvested by centrifugation (4600 rpm; 1min), frozen at −80°C, and lysed using zirconia beads. RNA was extracted using phenol:chloroform, and residual DNA was degraded by treatment with Turbo DNase (ThermoFisher Cat#AM2238) in a 50 μL reaction consisting of 10–25 μg of RNA, 1 U DNase, and 20 U of RNasIN in a 1X solution of the manufacturer-supplied buffer at 37°C for 30 min. Subsequently, the DNase was removed by phenol-chloroform extraction followed by ethanol

precipitation. Reverse transcription (RT) and qPCR were performed using the Luna Universal one-step RT-qPCR kit (NEB Cat#E3005S) in a 5 μL reaction consisting of 300 pmol primers, 1X reaction mix, 1X enzyme mix, and 8.75 ng of RNA. Reaction mixtures were incubated in a thermocycler with an initial RT reaction (55°C for 10 min) followed by 40 cycles of amplification (95°C for 5s and 60°C for 10s).

QUANTIFICATION AND STATISTICAL ANALYSIS

Phylogenetics and protein domain analysis

Candidate Mrn1 and Nab6 homologs were identified using PSI-BLAST, and then confirmed using a reciprocal PSI-BLAST search against the *S. cerevisiae* genome. Sequence alignments were performed using ClustalW and phylogenetic trees were generated using MEGA11 (Maximum Likelihood Trees with default settings). Protein domains were predicted using SMART (http://smart.embl-heidelberg.de/) and NCBI's Conserved Domains tool. The RRM structures were aligned using the super command in PyMOL.

CRAC analysis

Bioinformatic analysis of CRAC datasets was performed as previously described.[21] Multiplexed CRAC datasets were separated using pyBarcodeFilter from the pyCRAC package.[47] Subsequently, Flexbar v3.4.0 [48] was used to remove sequencing adapters, trim low-quality baes from the 3′ end, and remove low-quality reads (parameters -ao 4 -u 2 -q TAIL -m 14 -at RIGHT with adapter sequence TGGAATTCTCGGGTGCCAAGGC. In addition to the barcode, each read contained three random nucleotides at the 5′ end to allow PCR duplicates to be collapsed using pyFastqDuplicateRemover.[47] Reads were filtered to exclude low-entropy sequences using bbduk (https://sourceforge.net/projects/bbmap/) (parameters: entropy = 0.65 entropywindow = 10 entropyk = 5). Subsequently, the reads were mapped to a modified version of the *S. cerevisiae* EF4.74 genome (Ensembl) in which the introns had been bioinformatically removed.[21] Sequencing reads were aligned using Novoalign v2.07.00, with reads mapping to multiple locations randomly assigned (-r Random). Reads which aligned to the same coordinates and had identical 5′ random barcodes were collapsed into a single read.

Genome coverage maps were generated using genomecov from bedtools v2.27.0 [48] and visualized using the Integrated Genomics Viewer.[46] The number of reads mapping to different mRNAs was tabulated using pyReadCounters[47] and a custom genome annotation file. Scatterplots were made using GraphPad Prism 9. Gene ontology area maps were generated using the Proteomaps website.[51] GO enrichment analysis was performed using GOrilla.[50] Bar graphs depicting CRAC data show the average of two replicates. Error bars represent SD. Further details can be found in the figure legends.

RNA-seq analysis

Paired-end reads were aligned to the intronless *S. cerevisiae* genome using STAR[45] and tabulated using featureCounts.[52] Genome coverage files were generated using genomecov from bedtools and scaled by fragments per million. For all analyses, we used the top 5000 transcripts, defined by their average expression across all replicates and conditions. Expression was measured using FPKM (fragments per kilobase per million) in order to account for differences in library depth. Volcano plots and PCA were performed using R with DESeq2[53] and ggplot2 and visualized using GraphPad Prism. The clustering analysis was performed on $\log_2$ transformed data using Morpheus (https://software.broadinstitute.org/morpheus) (settings: Euclidean distance, 8 clusters). Bar graphs depicting RNA-seq data show the average of two replicates. Error bars represent SD. The scatterplots in Figures 3C and 3D show values for individual genes and the overall mean. Statistical significance was calculated using a two-tailed t test without testing for normality. Further details can be found in the figure legend.

qPCR

Each sample was measured in technical quadruplicate and the results were averaged together. Relative expression was calculated using $\Delta\Delta C_t$ and by normalizing to the levels of *RPL6B* mRNA (reporter experiments) or 25S rRNA (thiolutin experiments) in each sample. Bar graphs show the average of at least two replicates and error bars show SD or SEM. Detailed information is provided in the figure legends.

Cell Reports, Volume *42*

Supplemental information

A posttranscriptional pathway regulates cell wall mRNA expression in budding yeast

Stefan Bresson, Vadim Shchepachev, and David Tollervey

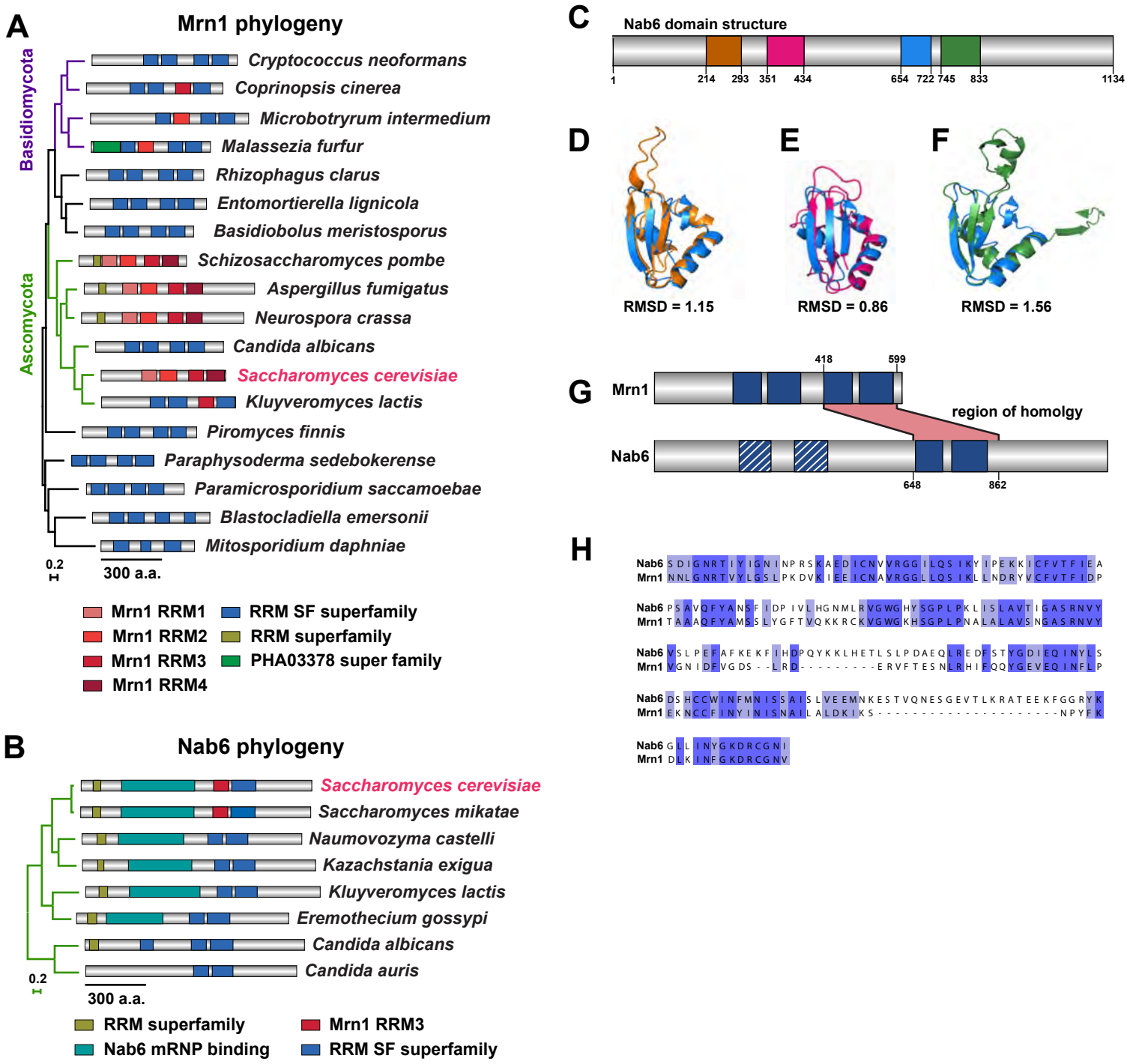

Figure S1

Figure S1. Evolutionary analysis of Mrn1 and Nab6. Related to Figure 1.
(A-B) Phylogenetic trees and NCBI-predicted domain structures for Mrn1 (A) and Nab6 (B) across fungi. Branch lengths are expressed in units of substitutions per site. A scale bar is shown below each tree. (C) Predicted domain architecture of Nab6 based on analysis of the Alphafold structure. Each RRM shown in a different color. RRM1: 214-293 (orange). RRM2: 351-434 (pink). RRM3: 654-722 (blue). RRM4: 745-833 (green). (D-F) Structural alignments of RRM3 with RRM1 (B), RRM2 (C), and RRM4 (D). The colors are the same as in (A). (G) Domain architecture of Mrn1 and Nab6. Two putative RRMs identified visually using Alphafold are shown in blue with white stripes. The region of homology between Mrn1 and Nab6 is indicated in pink. (H) Sequence alignment of the region of homology between Mrn1 and Nab6. Identical residues are shown in dark blue, and similar residues are shown in light blue.

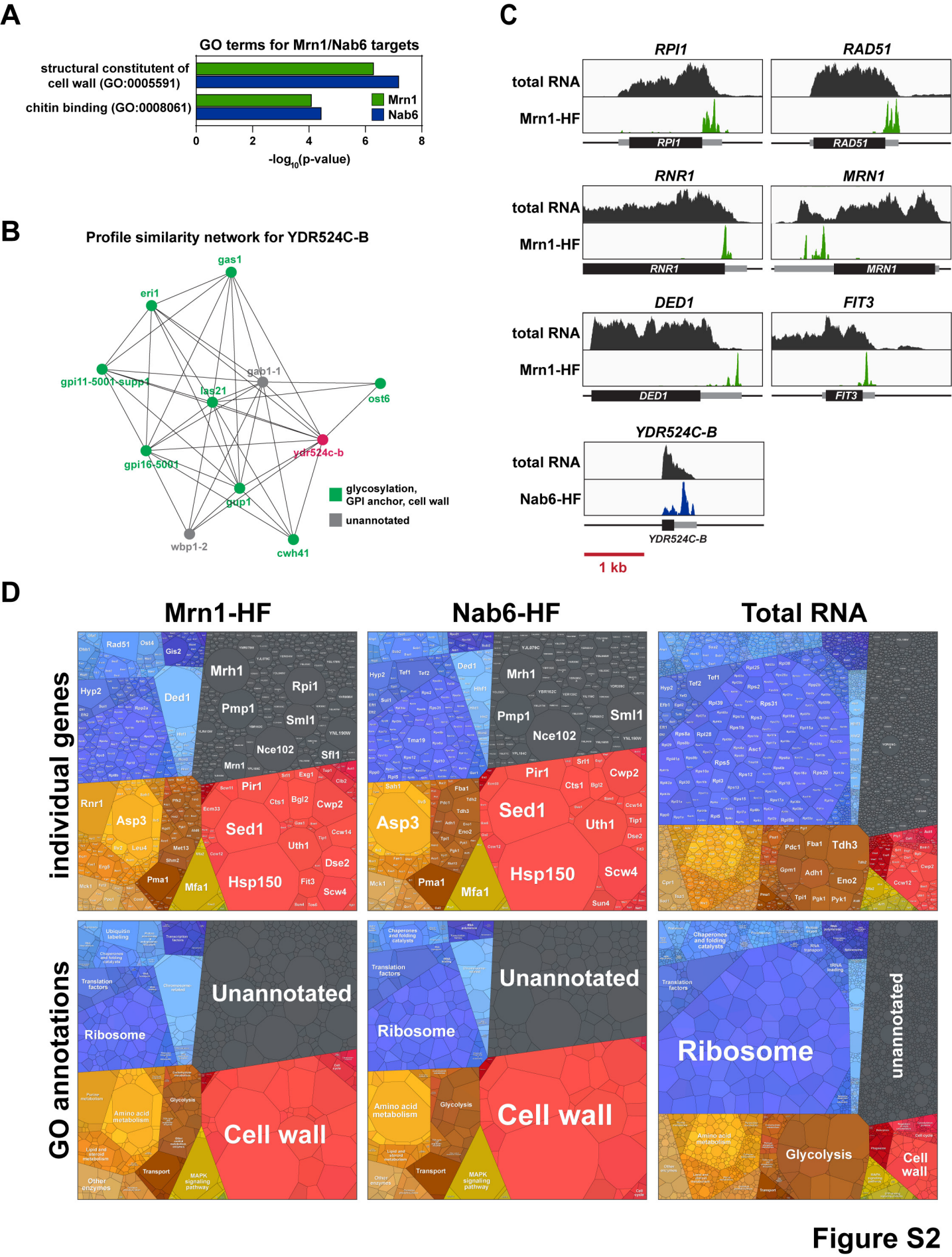
A
GO terms for Mrn1/Nab6 targets
structural constitutent of cell wall (GO:0005591)
chitin binding (GO:0008061)
Mrn1
Nab6
0
2
4
6
8
-log10(p-value)
B
Profile similarity network for YDR524C-B
gas1
eri1
gpi11-5001-supp1
gab1-1
las21
ost6
ydr524c-b
gpi16-5001
gup1
wbp1-2
cwh41
glycosylation, GPI anchor, cell wall
unannotated
C
RPI1
RAD51
RNR1
MRN1
DED1
FIT3
YDR524C-B
total RNA
Mrn1-HF
Nab6-HF
1 kb
D
Mrn1-HF
Nab6-HF
Total RNA
individual genes
GO annotations
Unannotated
Ribosome
Cell wall
Amino acid metabolism
Glycolysis
Transport
MAPK signaling pathway
Other enzymes
unannotated

Figure S2

Figure S2. Gene-ontology analysis of Mrn1 and Nab6 target mRNAs. Related to Figure 1. (A) GO-enrichment analysis for Mrn1 and Nab6 target genes. (B) Genetic profile similarity map for YDR524C-B showing genes with related sets of genetic interactions. Genes with a known role in cell wall biogenesis are marked in green. (C) Binding of Mrn1 and Nab6 across selected target transcripts preferentially targeted by one protein or the other. Each track is normalized to total library size using reads per million. RNAseq reads are included as a control. Each box represents a 3 kb window; a scale bar is shown at the bottom. The open reading frames (ORFs) are shown as black boxes, with UTRs as flanking gray boxes. Each transcript is oriented 5′ to 3′. (D) Area plots showing the proportion of each library mapping to individual genes. The upper panels show individual genes, and the lower panels show GO terms. Note that because of the way the data is represented, multifunctional genes can only be assigned to a single GO term. ASP3, for example, is both a structural component of the cell wall and a metabolic gene, but is only annotated as the latter.

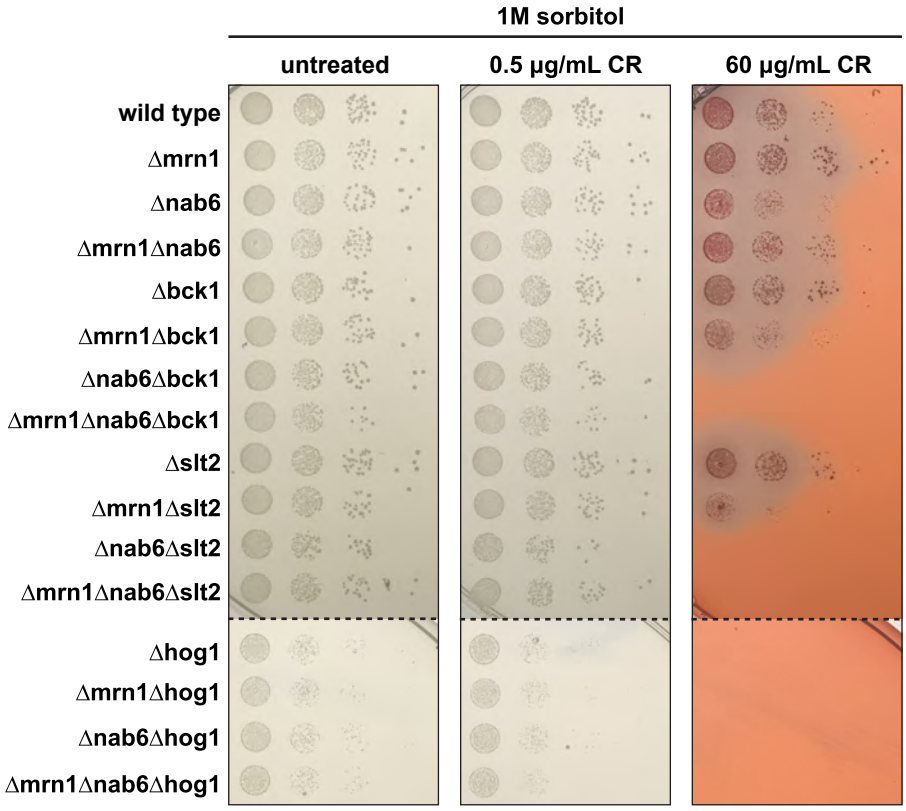

Figure S3

Figure S3. Sorbitol rescues the hypersensitivity of *Δnab6ΔCWI* strains to Congo red. Related to Figure 2.
Strains with combinations of gene deletions were tested for their ability to grow on plates with 0.5 µg/mL and 60 µg/mL Congo red supplemented with 1 M sorbitol. Cells were grown for two days at 30°C.

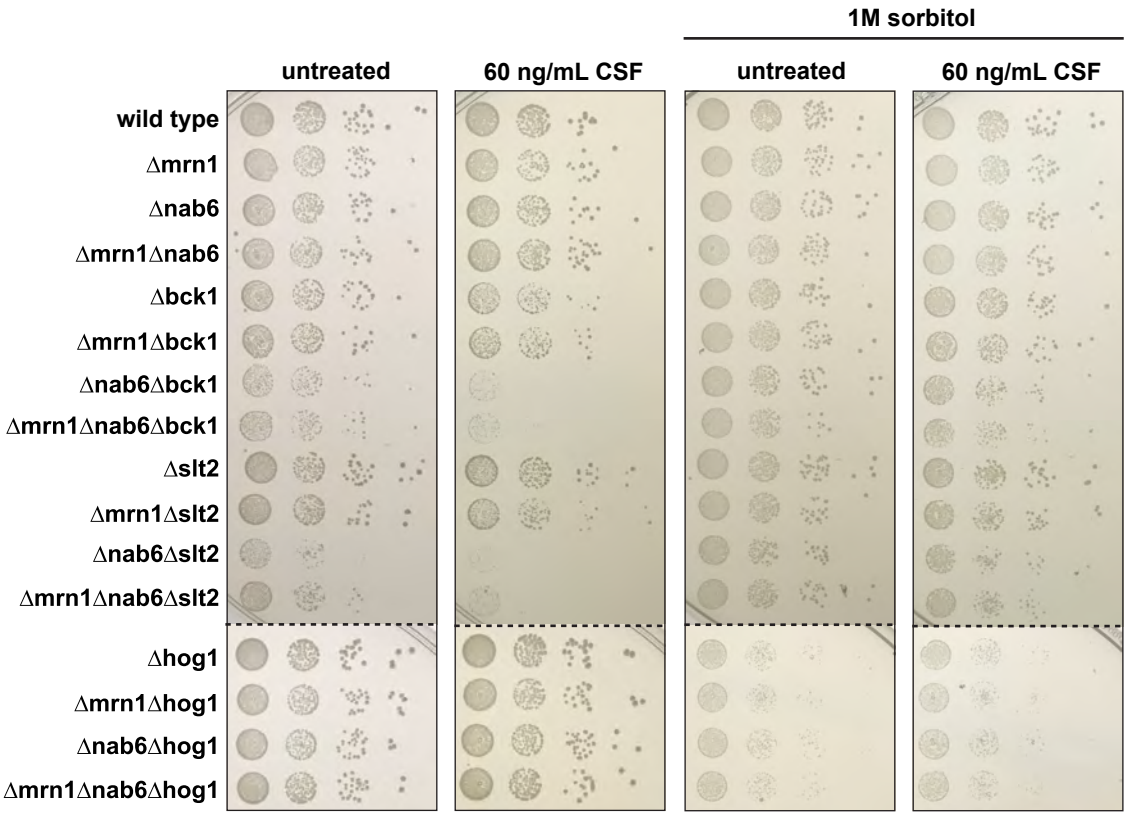

Figure S4

Figure S4. *Δnab6ΔCWI* strains are hypersensitive to caspofungin. Related to Figure 2. Strains with combinations of gene deletions were tested for their ability to grow on plates supplemented with 60 ng/mL caspofungin (CSF) and with or without addition of 1 M sorbitol. Growth assays for cells on plates lacking CSF are included for comparison (identical to the images in Figs. 2B and S3). Cells were grown for two days at 30°C.

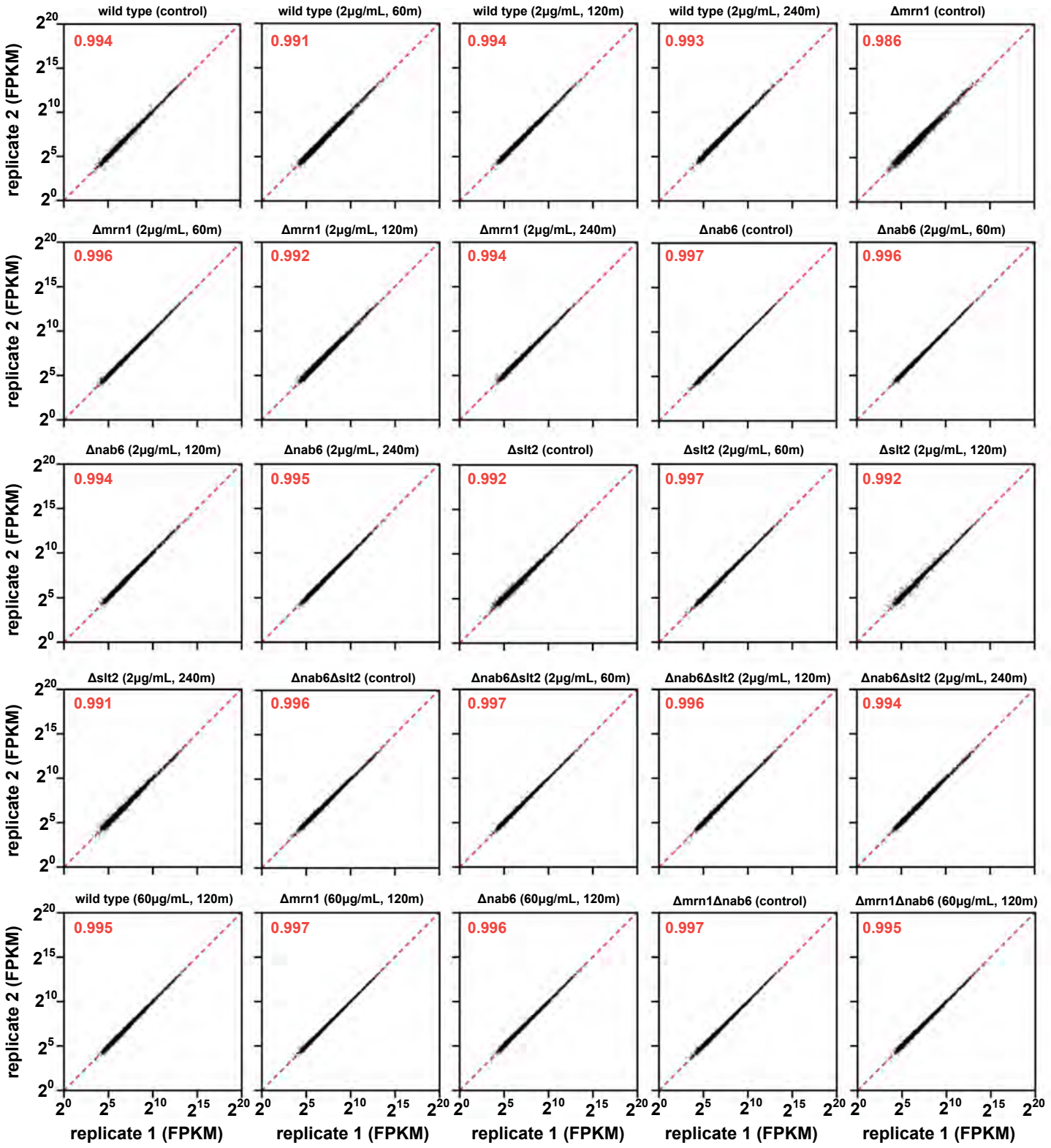

Figure S5

Figure S5. Reproducibility of RNAseq libraries. Related to Figure 3.

Comparison of RNAseq replicate datasets for 5,000 mRNAs plotted by FPKM (fragments per kilobase per million). The red number indicates the Spearman correlation coefficient.

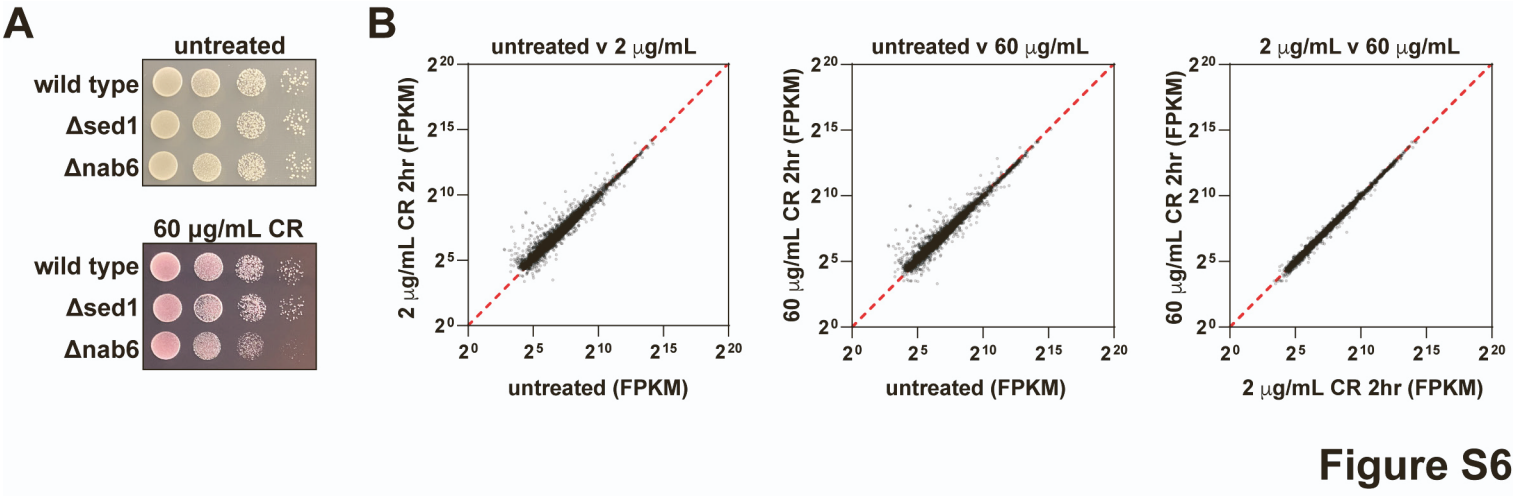

Figure S6

Figure S6. Comparison of gene expression changes in response to different concentrations of CR. Related to Figure 3.
(A) Wild type, Δsed1, and Δnab6 strains were tested for their ability to grow on 60 μg/mL Congo Red. Cells were grown for two days at 30°C. (B) Scatter plots showing comparisons between different RNAseq datasets for the wild type strain. FPKM (fragments per kilobase per million).

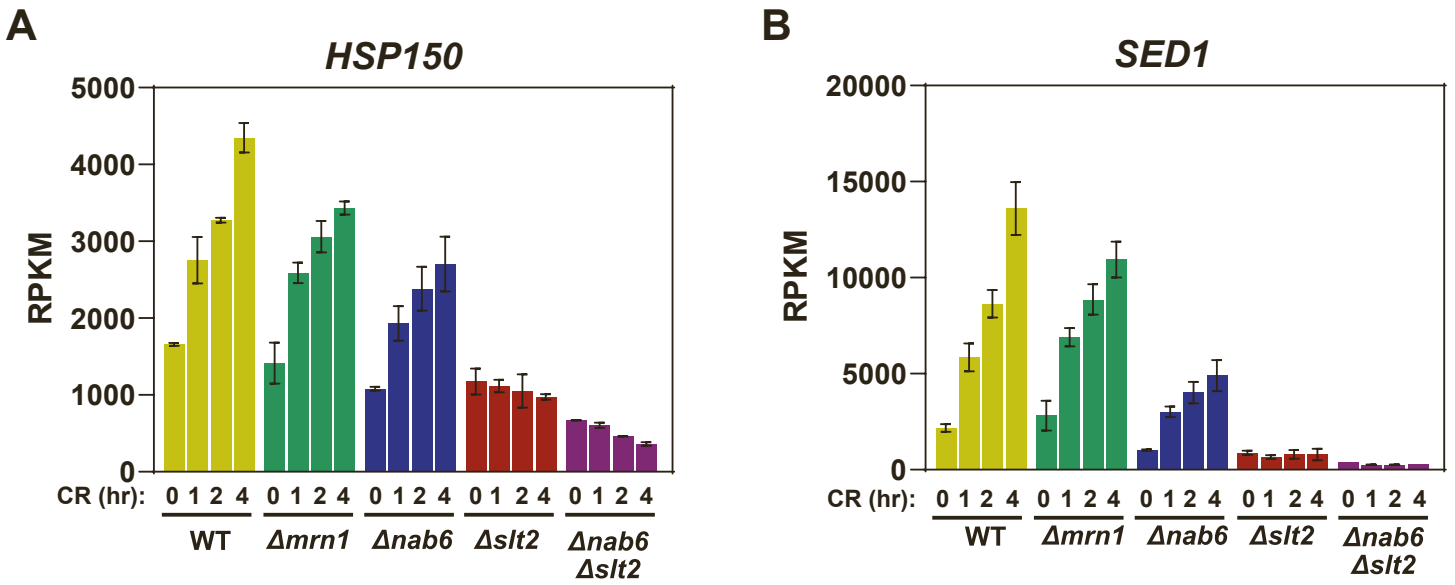

Figure S7

Figure S7. *HSP150* and *SED1* mRNA levels are altered following loss of Nab6 and/or Slt2. Related to Figure 3.
(A-B) Bar graphs showing changes in (A) *HSP150* and (B) *SED1* mRNA abundance following CR treatment. RPKM: reads per kilobase per million mapped reads.

plasmid name	description	purpose
pSB045	pML104 Slt2 gRNA	gene deletion
pSB046	pML104 Bck1 gRNA	gene deletion
pSB054	pML104 Nab6 gRNA	C-terminal HF tagging and gene deletion
pSB055	pML104 Mrn1 gRNA	C-terminal HF tagging and gene deletion
pSB091	pALD6-Venus-tSED1	MoClo Cassette
pSB098	pSED1-Venus-tADH1	MoClo Cassette

Table S4. Plasmids generated for this project. Related to STAR methods.

standard strains		
strain name	**description**	**background**
ySB125	Nab6-HF	BY4741
ySB126	Mrn1-HF	BY4741
ySB155	Δmrn1	BY4741
ySB158	Δslt2	BY4741
ySB159	Δbck1	BY4741
ySB160	Δnab6	BY4741
ySB162	Δmrn1Δnab6	BY4741
ySB163	Δmrn1Δbck1	BY4741
ySB164	Δmrn1Δslt2	BY4741
ySB165	Δhog1	BY4741
ySB166	Δmrn1Δhog1	BY4741
ySB167	Δnab6Δhog1	BY4741
ySB168	Δmrn1Δnab6Δhog1	BY4741
ySB169	Δnab6Δslt2	BY4741
ySB170	Δnab6Δbck1	BY4741
ySB171	Δmrn1Δnab6Δslt2	BY4741
ySB172	Δmrn1Δnab6Δbck1	BY4741
ySB224	Δsed1	BY4741

reporter constructs							
strain name	**background**	**cassette**	**promoter**	**CDS**	**terminator**	**selectable marker**	**integration site**
ySB193	wild type (BY4741)	pSB091	pALD6	Venus	tSED1	HygR	HO
ySB195	wild type (BY4741)	pSB098	pSED1	Venus	tADH1	HygR	HO
ySB198	Δmrn1 (ySB155)	pSB091	pALD6	Venus	tSED1	HygR	HO
ySB200	Δmrn1 (ySB155)	pSB098	pSED1	Venus	tADH1	HygR	HO
ySB203	Δnab6 (ySB160)	pSB091	pALD6	Venus	tSED1	HygR	HO
ySB205	Δnab6 (ySB160)	pSB098	pSED1	Venus	tADH1	HygR	HO
ySB208	Δslt2 (ySB158)	pSB091	pALD6	Venus	tSED1	HygR	HO
ySB210	Δslt2 (ySB158)	pSB098	pSED1	Venus	tADH1	HygR	HO
ySB213	Δmrn1Δnab6 (ySB162)	pSB091	pALD6	Venus	tSED1	HygR	HO
ySB215	Δmrn1Δnab6 (ySB162)	pSB098	pSED1	Venus	tADH1	HygR	HO

Table S5. Yeast strains generated for this project. Related to STAR methods.

gene	purpose	sequence
SLT2	CRISPR gRNA for gene deletion FWD	GATCGTTGACCGGATTTGATGATTGTTTTAGAGCTAG
SLT2	CRISPR gRNA for gene deletion REV	CTAGCTCTAAAACAATCATCAAATCCGGTCAAC
SLT2	homologous repair template for gene deletion FWD	CTATCAAAATAGTAGAAATAATTGAAGGGCGTGTATAACAATTCTGGGAGGACAAAAAAC
SLT2	homologous repair template for gene deletion REV	TTACATCTATGGTGATTCTATACTTCCCCGGTTACTTATAGTTTTTTGTCCTCCCAGAAT
BCK1	CRISPR gRNA for gene deletion FWD	GATCATATGTTGCTGGTGGCTCCGGTTTTAGAGCTAG
BCK1	CRISPR gRNA for gene deletion REV	CTAGCTCTAAAACCGGAGCCACCAGCAACATAT
BCK1	homologous repair template for gene deletion FWD	TAGTACGAAACACTAAATATAGTATTAAAATAGTTCAACTCCACCTCCAACTATTAGGAT
BCK1	homologous repair template for gene deletion REV	TATATTATTACGTATGCATAAATATCTTAAGTATAGATCGATCCTAATAGTTGGAGGTGG
NAB6	CRISPR gRNA for gene deletion FWD	GATCCAATATTTTGGGCGCCTCTGGTTTTAGAGCTAG
NAB6	CRISPR gRNA for gene deletion REV	CTAGCTCTAAAACCAGAGGCGCCCAAAATATTG
NAB6	homologous repair template for C-terminal HF-tagging FWD	AATATTTTGGGCGCCTCTGCAGAAGACAACACGCATCCTGACGAGCATCACCACCATCATCACCATCACGCCGCAGCCGCAGATT
NAB6	homologous repair template for C-terminal HF-tagging REV	TCCGATGGATATGCATTATACTTCAGGCTCAGCACAGCTATACTACTTGTCATCGTCATCTTTATAATCTGCGGCTGCGGCGTGA
NAB6	homologous repair template for gene deletion FWD	ACAAGACTCGCAAGAATCCGTTTTCTATTGTTTTTTTTGAGGATTCCAATTATAGCTGTG
NAB6	homologous repair template for gene deletion REV	CTAAATAGTCCGATGGATATGCATTATACTTCAGGCTCAGCACAGCTATAATTGGAATCC
MRN1	CRISPR gRNA for gene deletion FWD	GATCTACATAATGTTTAACGTGATGTTTTAGAGCTAG
MRN1	CRISPR gRNA for gene deletion REV	CTAGCTCTAAAACATCACGTTAAACATTATGTA
MRN1	homologous repair template for C-terminal HF-tagging FWD	AACTTTGGCAAGGATAGATGTGGTAACGTCCCCCATCAATCACGTCATCACCACCATCATCACCATCACGCCGCAGCCGCAGATT
MRN1	homologous repair template for C-terminal HF-tagging REV	ACTAAACATCTACGTACATACATATACATATATACATAATGTTTACTTGTCATCGTCATCTTTATAATCTGCGGCTGCGGCGTGA
MRN1	homologous repair template for gene deletion FWD	GTATTTTTTTTTTTCTTCACCATCACATACTACTTCAATTGCATTAAAACACATTATGTA
MRN1	homologous repair template for gene deletion REV	AGACGGACACTAAACATCTACGTACATACATATACATATATACATAATGTGTTTTAATGC
HOG1	homologous repair template for gene deletion and replacement with HIS3 FWD	AAAAAGGAACAAAGGGAAAACAGGGAAAACTACAACTATCGTATATAATACGGATCCCCGGGTTAATTAA
HOG1	homologous repair template for gene deletion and replacement with HIS3 REV	ACATCAAAAAGAAGTAAGAATGAGTGGTTAGGGACATTAAAAAAACACGTGAATTCGAGCTCGTTTAAAC
SED1 promoter	part generation FWD	GCATCGTCTCATCGGTCTCAaacgTCCCCGAGAAAGCTTAG
SED1 promoter	part generation REV	ATGCCGTCTCAGGTCTCAcataGATCTCTTAATAGAGCGAACGTATTTTATTTTG
SED1 terminator	part generation FWD	GCATCGTCTCATCGGTCTCAatccTAACTCaAGACGGTGGTGTTTGACAC
SED1 terminator	part generation REV	ATGCCGTCTCAGGTCTCAcagcAAATACTTTCATGAAGCACTAGAAAAAAC
Venus	qPCR FWD	GTCTCCGGTGAAGGTGAAGG
Venus	qPCR REV	AAGGTTGGCCATGGAACTGG
RPL6B	qPCR FWD	GCTGCCCCAAAGAAAACCAG
RPL6B	qPCR REV	GCCTGGAACTAGAGAGGCAC
SED1	qPCR FWD	TTGAAAAGAGCGAAGCCCCT
SED1	qPCR REV	CGGTTAGACTTGGGTTGGCT
25S rRNA	qPCR FWD	CGCGGTGATTTCTTTGCTCC
25S rRNA	qPCR REV	TAGCCTGCTATGGTTCAGCG

Table S6. Oligonucleotides used in this project. Related to STAR methods.